Heimo Tuovinen and Per Blomqvist

Modelling of Hydrogen Cyanide Formation in Room Fires

BRANDFORSK project 321-011

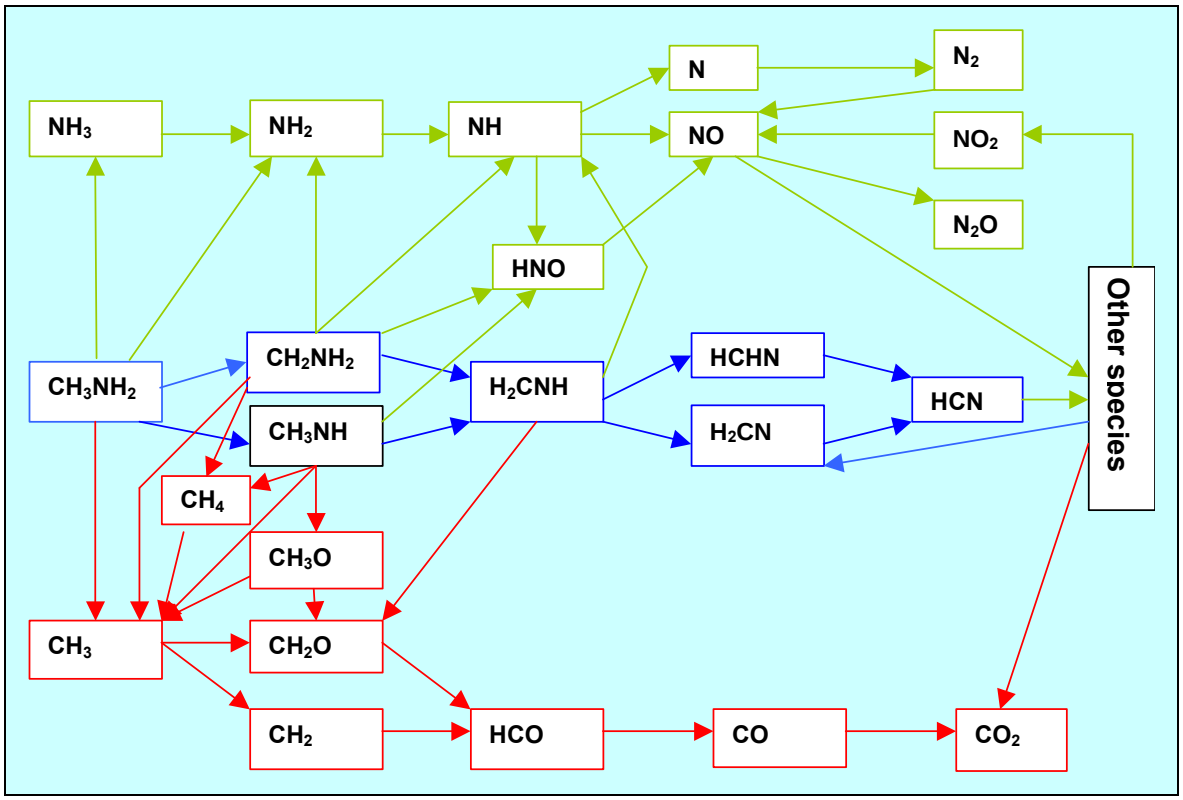

Abstract

A chemical kinetics model for calculation of the formation of hydrogen cyanide (HCN) has been made. The combustion of two mixtures with different ratios of methylamine and ethylene has been modelled using the laminar flamelet concept. The flamelet calculations are based on several thousand elementary reaction steps to describe the chemical kinetics of HCN in combustion. The flamelets for both cold (293 K) and hot (1000 K) combustion product recycling have been calculated. The effect of strain is also included in the calculations. Scalar dissipation rates from 0.01s to extinction values have been varied.

Separate flamelet sets for various levels of radiation, from adiabatic up to 30 % radiation losses, incremented by 1%, have been made. In the flow field calculation the flamelet options may be used either as adiabatic, constant radiation or an interpolation between flamelet sets of different radiation.

The chemical kinetics model incorporated into CFD code has been used to simulate two laboratory fire tests of the combustion of nylon. Changing the size of the opening in the test room varied the ventilation. The calculated flamelet sets for the mixture of methylamine and ethylene, with nitrogen content close to that of nylon, were used in these simulations. The simulations were made with and without recycling the combustion products back to the fire.

The calculations show that recycling of the combustion products to the fire increases the formation of HCN and CO. Similarly, the lowered ventilation rate increases the formation of these species. The calculated temperatures and main species concentrations, including HCN, agree well with the laboratory measurements.

Key words: Flamelet models, hydrogen cyanide, CFD models, vitiation, under-ventilated fires

SP Sveriges Provnings- och Forskningsinstitut
SP Rapport 2002:10
ISBN 91-7848-941-5
ISSN 0284-5172
Borås 2003

SP Swedish National Testing and Research Institute
SP Report 2003:10

Postal address:
Box 857,
SE-501 15 BORÅS, Sweden
Telephone: +46 33 16 50 00
Telex: 36252 Testing S
Telefax: +46 33 13 55 02
E-mail: info@sp.se

Abstract **2**

Acknowledgements **4**

Sammanfattning **5**

Nomenclature **6**

1 Introduction **9**
1.1 Background 9
1.2 Combustion models 9
1.3 Combustion in vitiated air 10

2 CFD model SOFIE **11**

3 Laminar flamelet model for multi-component chemistry **13**
3.1 The laminar flamelet concept 13
3.2 Effect of strain, scalar dissipation 15
3.3 Radiation losses 15
3.4 Flamelet balance equations 15

4 Calculated flamelets **17**
4.1 Flamelet boundary conditions 17
4.2 The flamelet library 18
4.3 Implementation in CFD 19

5 Full scale validation data and design fires **23**
5.1 Fire tests used for initial validation of the model 23
5.2 Description of the design fires 24

6 CFD simulations **27**
6.1 Comparison with measurements 28
6.1.1 Gas temperatures 28
6.1.2 Species concentrations 29

7 Representation of the chemical kinetics **33**
7.1 H-atom abstraction 33
7.2 C-N bond scission 34
7.3 Formation of HCN 35
7.4 Main reaction paths to HCN formation 36
7.5 Destruction of HCN 38
7.6 Some aspects of nylon combustion 38

8 Discussion and Conclusion **41**

9 Future work **43**

10 References **45**

Appendix A **49**

Appendix B **53**

Acknowledgements

This work was supported by the Swedish Fire Research Board (BRANDFORSK Project 321-011), which is gratefully acknowledged. The authors would like to thank the Reference Group and especially Prof. Göran Holmstedt at the Department of Fire Safety Engineering, Lund University, for helpful discussions during the project.

Acknowledgements are also given to Dr. Fabian Mauss and Fikret Saric at the Division of Combustion Physics, Lund University, for calculation of flamelets.

Sammanfattning

En beräkningsmodell för bildning av vätecyanid (HCN) har tagits fram. Förbränning av två blandningar av metylamin och etylen har modellerats med s.k. laminar flamelet modell. Ett omfattande kemisk kinetiskt reaktionsschema bestående av flera tusen reaktioner har använts för att beräkna HCN kinetiken. Flamelet beräkningarna har utförts för återcirkulation av både kalla (293 K) och varma (1000 K) rökgaser tillbaka till branden. Inverkan av flamtöjning (eng. strain rate) och strålning från tunna flamfragment har också inkluderats.

Separata flameletuppställningar för olika strålningsvärden från adiabatiska upp till 30 % strålningsförluster med 1 % steg mellan strålningsnivåerna har beräknats. Flameletstrålning kan utnyttjas i CFD på flera olika sätt: som adiabatisk (strålningen försummat), fix strålning eller interpolation mellan flameletuppställningar med olika strålning.

Modellen har använts för att simulera två laboratorieprovningar av förbränning av nylon. Simuleringarna har utförts med två olika ventilationsförhållanden och med och utan återcirkulation av rökgaser till branden.

Beräkningarna visar att återcirkulation av förbränningsprodukter tillbaka till branden ökar bildning av både HCN och CO. Lägre ventilationsgrad medför också ökning av dessa ämnen. Beräknade temperaturer och koncentrationer av huvudreaktionsprodukter samt HCN stämmer relativt bra med laboratorietester.

Nomenclature

A	Area of opening
C_p	Heat capacity
c_{g1},c_{g2}	Empirical constants in k-ε model
$c_{\varepsilon 1}$,$c_{\varepsilon 2}$	Empirical constants in k-ε model
D	Diffusion coefficient
H	Height of opening
h_i	Enthalpy of specie *i*
k	Turbulent kinetic energy
Le	Lewis number
$\dot{m}$	Mass flow rate of air
M_i	Molecular weight of specie *i*
N	Number of species
$\widetilde{P}(\xi)$	Favre averaged pfd of mixture fraction
$\dot{Q}$	Heat release rate
$\dot{q}_R$	Radiation loss
r_o	Fuel to oxidiser ratio
t	Time
$\widetilde{u}_k$	Favre averaged velocity component in x_k direction
u_k''	Fluctuating component of velocity in x_k direction
T	Temperature
Y_F	Mass fraction of fuel
Y_i	Mass fraction of specie *i*
$Y_{F,1}$	Mass fraction of fuel in fuel stream
$Y_{O_2,2}$	Mass fraction of oxygen in oxidiser stream
α	Coefficient in heat release rate equation
α	Exponent in Beta function
β	Exponent in Beta function
Γ	Gamma function
ε	Dissipation of turbulent kinetic energy
ϕ	Scalar in flamelet model
Φ	Global equivalence ratio
ρ	Density
$\overline{\rho}$	Mean density (Reynolds averaged)
$\dot{\omega}$	Chemical production rate of specie *i*
ξ	Mixture fraction
$\widetilde{\xi}$	Favre averaged mixture fraction
ξ''^2	Mixture fraction variance
ν	Stoichiometric oxidiser-to-fuel ratio
σ	Prandtl/Schmidt number
μ	Viscosity
χ	Scalar dissipation rate
ψ	Vitiation fraction
ν_i'	Stoichiometric coefficient of specie *i* appearing as reactant
ν_i''	Stoichiometric coefficient of specie *i* appearing as product

Subscripts

lam	Laminar
tur	Turbulent
1	Fuel stream (stream1)
2	Oxidiser stream (stream 2)

1 Introduction

1.1 Background

Hydrogen cyanide (HCN) is formed in combustion of any nitrogen-containing materials. Emission of HCN from combustion of common materials used in our home environment has been measured in a previous BRANDFORSK project [1]. It was seen from this project that HCN was produced from all tested materials, preferably from pyrolysis and under conditions of restricted availability of oxygen.

HCN is about 35 times more toxic than carbon monoxide (CO). Further the influence of HCN on humans is quite difference to that of CO. HCN is carried rapidly to the brain by the blood, making the victim quickly incapacitated. The uptake rate is directly related to the concentration of HCN in the air the victim is breathing. As low as 20 ppm HCN in the air shows symptoms in victims after longer times exposure. Concentrations of 120-150 may be life-threatening after a half an hour and the concentrations of 3000 ppm (0.3 % by volume) may directly lead to death. Because of its high toxicity HCN is important in designing the evacuation routes from fires. The more detailed description of HCN on human is presented in reference [1].

To be able to investigate the production and spread of HCN with fire-induced flows in multi-room buildings CFD models should be used. Large scale fire tests are very expensive and it is almost impossible to make detailed measurements of HCN in as many points as necessary to estimate the pattern good enough to understand the spread of HCN.

For use in CFD validations the fuel must have well known burning properties and the combustion of it should be easy to control. To have such properties the fuel should be in the gas phase. It is difficult to find nitrogen-containing fuel that is in gas phase in room temperature. Therefore, we have decided to simulate burning nylon using a fictitious mixture of two fuels: ethylene and methylamine.

1.2 Combustion models

Combustion engineers in recent decades have been investigating the chemistry in several combustion systems, such as internal combustion engines, furnaces and jet engines. To calculate only the rate of heat release a simple chemical model can be used. In the simplest models the chemistry is assumed to occur as a one-step reaction in which the fuel is directly converted to combustion products. In many cases this is a reasonable approximation. However, in reality, thousands of chemical reactions are involved in the combustion and the combustion is not fully complete in any of the real combustion systems. It is well known that many combustion systems pollute our environment, emitting CO, NOx, etc. Thus, there has been a need to understand combustion in more detail to be able to reduce the formation of unwanted pollutants and assist in the design of more efficient combustion. This has lead to development of several combustion models for different applications.

There are two main combustion models that have become widely used in combustion simulations: eddy break-up [2] and the laminar flamelet models [3]. These two models have also become those most commonly used in the CFD models employed by fire safety engineers. The Eddy beak-up model is most commonly used in fire applications. The

laminar flamelet model has only been used for these applications for about the past 10 to 15 years, although it has been used in combustion science much longer.

1.3 Combustion in vitiated air

In room fires the oxygen content in the air that is entrained into the fire is usually lower than in fresh air. The air in the fire location usually also contains the products of combustion, i.e., the air is vitiated. This reduces the combustion efficiency and yields more products of incomplete combustion. Thus, to model the chemistry correctly the boundary conditions for flamelets must be modified to take the effect of vitiation on the chemistry into account. As the re-circulation varies as the fire grows so does the contents of combustion products in the air. There is, therefore, a need to calculate the flamelets for varying degrees of vitiation.

Depending on the ventilation conditions, fire size compared to room size and other burning conditions the recycled combustion products may be either hot or cold [4]. Therefore the flamelets should also be calculated using boundary conditions on the oxidant side for both cold and hot vitiation.

The flamelets calculated in a vitiated atmosphere have not been used very much to date. The first work of calculated flamelets in vitiated air was made in 1991 [4-6]. That work was conducted prior to connection of the flamelet model to CFD. The reaction mechanism was a simple 13-step scheme for methane as a fuel. A few years later these methane-air flamelets were implemented in the CFD model SOFIE [7,8].

The model was then further developed to include a more complex fuel, heptane. The reaction scheme consisted of about 2000 elementary reaction steps [9,10]. The chemistry of heptane consists of a large number of intermediate combustion products that better represent the situation in room fires.

The work presented in this project is a further development of the model to take the formation of hydrogen cyanide into account. The current model consist of several thousands chemical reactions and is based on two mixtures of methylamine and ethylene. The flamelet calculations carried out in this study used the so-called ‘Arc length Continuation Method’ [11], which solves a set of differential equations, including the inverse of scalar dissipation rate as a variable.

The increase of the chemical reaction scheme demands an increase in computer storage and computing time, of which the computing time is the limiting factor. Thus, the chemistry calculations are not convenient to perform at the same time as the flow field calculations. Even though we have fast computers today, the calculation of the chemistry at every node (control volume) at each time step, would take unrealistically long time. Thus, the modellers must find a way to reduce the calculation time. In this work the chemical kinetic calculations, due to the huge chemical reaction scheme involved to be calculated in several physical conditions such as varying vitiation, were removed from the flow field calculations. The pre-calculated flamelet state relationships were stored in so called flamelet libraries for use in flow field calculations with CFD.

2 CFD model SOFIE

SOFIE (Simulation Of Fires In Enclosures) has been available for fire researchers for the last decade. SOFIE has been developed at Cranfield University in UK with sponsorship from several leading fire laboratories in Europe including SP Swedish National Testing and Research Institute.

SOFIE employs most basic features needed for computation of fluid dynamics problems and several additional sub-models specifically related to fire and combustion simulations, such as combustion, turbulence, radiation, heat transfer and soot formation. The basic code includes several optional solvers.

Two widely used combustion models are: the Eddy break-up [2], modified by Magnussen [12], and the laminar flamelet model [3]. The $k - \varepsilon$ turbulence model with buoyancy production modification term is used for calculation of turbulence. For calculation of the radiation exchange between fluid and solid walls of the enclosure, a discrete transfer model (DTRM) [13] is available. Soot formation (nucleation, coagulation and surface growth) and oxidation can be modelled using Magnussen (Tesner) model or the Two-Scalar Transport model (flamelet source terms). Although it is a relatively new code, it has been successfully used to simulate fires in several types of enclosures [14-16].

In this project the laminar flamelet model has been developed further to calculate the formation of hazardous hydrogen cyanide (HCN) in flames, which is formed from nitrogen-containing fuels, especially during vitiated conditions.

3 Laminar flamelet model for multi-component chemistry

The laminar flamelet model has been a widely used combustion model in studying the combustion in various types of combustion systems, such as internal combustion engines, gas turbines and jet engines. It is now becoming established in the simulation of fires with CFD models. One “disadvantage” with the flamelet model when simulating fires is that it requires a very fine mesh in order to make accurate calculations in combustion regions. When simulating very large fire scenarios it needs a large number of cells, and hence large computer memory, which could be time consuming. This is a result of the very large number of chemical species that need additional memory in order to calculate their concentrations simultaneously.

However, one “advantage” with the laminar flamelet model is a special technique that is used to implement the chemical kinetics in CFD models: all the chemical components have been treated as derived variables, i.e. they are calculated as a fraction of one well known parameter, the mean density. Thus, it is not necessary to include all the components in the flow field calculation. This saves a lot of computer memory and calculation time, without loosing any important information.

Another advantage with the laminar flamelet model is that it appears to be a reliable model when taking chemical kinetics with very large number of components into account. It has been successfully used in a previous investigation of vitiated fires in which an approximately 2000-step chemical reaction mechanism containing approximately 100 species was considered [9].

3.1 The laminar flamelet concept

A laminar diffusion flame provides unique relationships for chemical species, temperature, and enthalpy and even for viscosity and soot concentration, in terms of a so-called conserved scalar [3]. A laminar diffusion flame also provides a good opportunity for measuring these relationships, using, for example, a counter-flow diffusion flame [17] or co-flow diffusion flame [3].

All the atoms in the chemically reacting flows, such as in diffusion flames or fires are conserved scalars, because they cannot be created or destroyed when taking part in the chemical reactions. Any of them could be used as a major parameter for describing the mixing of the fuel and oxidant streams. However, the most suitable choice of the conserved scalar in mixing of two flow streams (with or without combustion) is the mixture fraction.

One advantage of using the mixture fraction as a conserved scalar is that it is a simple function of the fuel always having value between zero (pure air) and unity (pure fuel). All species are very simple to express as a function of the mixture fraction rather than as a function of, for example, a carbon atom.

The mixture fraction states what fraction of the mixture originates from the fuel at any given point in the laminar flame sheet. In other words, there are unique state relationships for all thermochemical parameters in terms of the mixture fraction across a laminar flame.

Assuming that a turbulent diffusion flame consists of microscopic elements having a structure of an undisturbed laminar diffusion flame these state relationships for thermochemical parameters from laminar diffusion flames can be averaged for turbulent diffusion flames using an appropriate shape of the probability density function (pdf). Since the flamelet is very thin, it can be described using a one- dimensional set of transport equations.

Further assuming that chemical reactions occur only in these thin flame sheets (flamelets) and the chemical time scale is short compared to the diffusion and turbulent transport time scales the statistical uncertainties in a turbulent flow field can be decoupled from the complex multi-component reaction chemistry. As the reaction time is assumed to be short compared to mixing time, the instantaneous species concentrations, thermochemical parameters and temperature are functions of the mixture fraction only, i.e.,

$$\phi = \phi(\xi) \tag{3.1}$$

where ϕ denotes any scalar variable. Here, a formal coordinate transformation has been made, using a conserved property of the turbulent reacting flow as an independent variable, which leads to a universal description of the flamelet properties. Introducing a Lagrangian co-ordinate system attached to a maximum-reaction rate surface, with the mixture fraction taken as an independent variable, performs the coordinate transformation. The mixture fraction is then defined as

$$\xi = \frac{\nu Y_F - Y_{O_2} + Y_{O_2,2}}{\nu Y_{F,1} + Y_{O_2,2}} \tag{3.2}$$

where ν is a stoichiometric oxidiser-to-fuel ratio, Y_i denotes the mass fraction of species i. The fuel is denoted by index F while O_2 denotes oxygen. The indices 1 and 2 denote initial fuel and initial oxidiser streams, respectively. The stoichiometric mixture fraction ξ_{st} can be expressed as

$$\xi_{st} = \left(1 + \frac{\nu'_{O_2} M_{O_2} Y_{F,1}}{\nu'_F M_F Y_{O_2,2}}\right)^{-1} \tag{3.3}$$

where ν'_{O_2} and ν'_F are the stoichiometric coefficients for oxygen and fuel, respectively, and M_{O_2} and M_F are molecular masses for oxygen and fuel, respectively. Using the expression for the oxidiser to fuel ratio r_o equation (3.3) becomes

$$\xi_{st} = \left(1 + \frac{r_o}{Y_{O_2,2}}\right)^{-1} \tag{3.4}$$

3.2 Effect of strain, scalar dissipation

The turbulence affects the flame sheets by stretching them and hence making them thinner, which affects the chemical reaction rate. Thus, the local hydrodynamic strain field influences the flamelet profiles. To take strain rate into account the flamelet profiles must be supplemented by information about the local strain field, i.e.,

$$\phi = \phi(\xi, \chi) \tag{3.5}$$

where χ denotes the scalar dissipation defined as

$$\chi = 2D \frac{\partial \xi}{\partial x_k} \frac{\partial \xi}{\partial x_k} \tag{3.6}$$

where D is the diffusion coefficient. The scalar dissipation is proportional to the inverse of the strain field. The value of χ can also be used as a measure of the instantaneous rate of molecular heat and mass transfer from the flamelet.

Including the scalar dissipation into the flamelet profiles tremendously increases the size of the flamelet database, because the flamelet state relationships as a function of the conserved scalar and the scalar dissipation are to be stored. However, the detailed chemical kinetics, including the effect on strain, can be incorporated into CFD models without an inordinate increase in computer time.

3.3 Radiation losses

The flamelets lose energy due to radiation to cooler surrounding gas. As in the reaction zone the temperature is about 2000 K or more, depending of the fuel, and as the radiation is proportional to the fourth power of the temperature, the radiation losses are considerable. The radiation losses tend to reduce the temperature of the flame sheet, which in turn affects the chemistry reducing the reaction rates.

3.4 Flamelet balance equations

Assuming a thin reaction zone and fast chemistry, it was shown by Peters [18] that in a steady state situation, temperature and species are determined by the balance between diffusion and chemical reactions as

$$\rho \frac{\chi}{2} \frac{d^2 T}{d\xi^2} = \frac{1}{C_p} \sum_{i=1}^{N} \dot{\omega}_i h_i + \dot{q}_R \tag{3.7}$$

and

$$\rho \frac{1}{Le_i} \frac{\chi}{2} \frac{d^2 Y_i}{d\xi^2} = -\dot{\omega}_i , \qquad \text{i = 1, 2…, N} \qquad (3.8)$$

where ρ is the mass density, $\dot{\omega}_i$ is the chemical production rate of specie *i*, h_i is the enthalpy of specie *i*, C_p is the heat capacity, Y_i is mass fraction of specie *i,* Le_i is the Lewis number and $\dot{q}_R$ is the radiation loss term. The Lewis number, denoting the ratio of energy- and mass-transport rates, is assumed to be unity. The equations (3.7) and (3.8) are solved numerically for various scalar dissipation rates and equivalence ratios.

4 Calculated flamelets

The flamelets are calculated for two different mixtures of methylamine and ethylene in pure air and the mixture of pure air and main combustion products. The effects of radiation and strain rate are included into flamelets.

The two fuel mixtures are chosen to vary the nitrogen content in the fuel, which yields different levels of HCN in the combustion. The following proportions of the two fuels are used in each mixture:

- Mixture 1: ethylene/methylamine ratio 3
- Mixture 2: ethylene/methylamine ratio 12

In mixture 1 the nitrogen content is about that of nylon (12.2 % by weight), which will yield high concentration of HCN in combustion. In mixture 2 the nitrogen content is lower, approximately the same level as in particleboard (3.8 % by weight).

4.1 Flamelet boundary conditions

The flamelets are calculated for various degrees of vitiation, i.e. fire gas re-circulation, which means that the oxidiser stream is mixed by a fraction of re-circulated combustion products. Only the main products of combustion (H_2O and CO_2) are re-circulated. The flamelet sets for both cold and hot vitiations are calculated. In cold vitiation the temperatures of both fuel and air streams are held at 293 K. In the hot vitiation the fire gases are assumed to have temperature of 1000 K. The temperature of vitiated air is calculated as the arithmetic mean values of hot gas at 1000 K and air at 293 K (equal heat capacities for hot gas and air assumed). The temperatures of oxidizer streams for different degrees of hot vitiation are shown in table 4.1.

Table 4.1 Oxidiser stream temperatures at various vitiation fractions for hot vitiation. The vitiation gas consists of stoichiometric proportions of the main combustion products, H_2O and CO_2, at 1000 K mixed with pure air at 293 K.

Vitiation fraction	Oxidiser temperature [K]
0	293
0.05	328
0.10	364
0.15	399
0.20	434
0.30	505
0.40	576
0.50	647
0.60	717

Species concentrations in the oxidiser stream vary due to vitiation. This affects the chemistry reducing the combustion efficiency, which leads to the generation of more products of incomplete combustion such as CO and HCN. The mole fractions of species in the oxidiser stream at various vitiation fractions are shown in tables 4.2 and 4.3.

Table 4.2 Mole fractions of species in oxidiser stream at various vitiation fractions for Mixture 1

Vitiation fraction	X_{O_2}	X_{N_2}	X_{CO_2}	X_{H_2O}
0	0.21	0.79	0	0
0.05	0.1995	0.7872	0.0060	0.0073
0.10	0.1890	0.7844	0.0120	0.0146
0.15	0.1785	0.7816	0.0180	0.0219
0.20	0.168	0.7788	0.0240	0.0292
0.30	0.147	0.7733	0.0360	0.0437
0.40	0.126	0.7677	0.0480	0.0583
0.50	0.105	0.7621	0.0600	0.0729
0.60	0.084	0.7565	0.0720	0.0875

Table 4.3 Mole fractions of species in oxidiser stream at various vitiation fractions for Mixture 2

Vitiation fraction	X_{O_2}	X_{N_2}	X_{CO_2}	X_{H_2O}
0	0.21	0.79	0	0
0.05	0.1995	0.7873	0.0064	0.0068
0.10	0.1890	0.7847	0.0128	0.0135
0.15	0.1785	0.7820	0.0192	0.0203
0.20	0.168	0.7794	0.0255	0.0271
0.30	0.147	0.7741	0.0383	0.0406
0.40	0.126	0.7688	0.0511	0.0541
0.50	0.105	0.7635	0.0638	0.0677
0.60	0.084	0.7582	0.0766	0.0812

4.2 The flamelet library

The flamelets for HCN generating fuels have been added to the existing flamelet library in SOFIE. The flamelet calculations were performed by Lund University, the Division of Combustion Physics. The method used is the so-called Arch length Continuation Method that solves the differential equations including the inverse of scalar dissipation rate as a variable. The scalar dissipation rate is calculated from low values, 0.04 s^{-1}, to extinction values. The number of flamelet sets in the flamelet library is therefore very large.

The flamelets are calculated for a non-vitiated oxidiser stream and for 8 levels of both cold and hot vitiation in the oxidiser stream (see tables 4.2 and 4.3) for two mixtures of fuel, i.e. totally 34 configurations. Each of these configurations includes a separate sub-library of flamelets consisting of 30 values of strain rate (scalar dissipation) and for every strain rate 30 sets of flamelets for varying radiation. Thus, the total number of flamelet sets is $34 \times 30 \times 30 = 30\ 600$.

4.3 Implementation in CFD

Coupling the calculated laminar flamelet data to a turbulent flow field requires information of the statistical distribution of the mixture fraction and the scalar dissipation. These parameters are to be calculated. Due to turbulence and the non-linear relationship between thermo-chemical parameters and the mixture fraction, information about the statistical fluctuation in the mixture fraction is required. The statistical fluctuation information is supplied in the form of a probability density function (pdf). In SOFIE the pdf is prescribed in the form of beta function,

$$\widetilde{P}(\xi) = \frac{\xi^{\alpha-1}(1-\xi)^{\beta-1}}{\int_0^1 \xi^{\alpha-1}(1-\xi)^{\beta-1} d\xi} = \frac{\Gamma(\alpha)\Gamma(\beta)}{\Gamma(\alpha+\beta)} \tag{4.1}$$

where tilde, "~", denotes the Favre-averaged quantities, Γ is a gamma function and variables α and β are calculated from the first two moments of the mixture fraction distribution, the Favre-averaged mixture fraction mean, $\widetilde{\xi}$, and its variance, $\widetilde{\xi}^{"2}$ according to:

$$\alpha = \widetilde{\xi}\left(\frac{\widetilde{\xi}(1-\widetilde{\xi})}{\widetilde{\xi}^{"2}} - 1\right) \tag{4.2}$$

and

$$\beta = \frac{\alpha(1-\widetilde{\xi})}{\widetilde{\xi}} \tag{4.3}$$

The moments are determined through solving the transport equations for both the mixture fraction mean and the variance:

$$\frac{\partial}{\partial t}(\overline{\rho}\widetilde{\xi}) + \frac{\partial}{\partial x_k}(\overline{\rho}\widetilde{u}_k\widetilde{\xi}) = \frac{\partial}{\partial x_k}\left\{\left[\frac{\mu_{lam}}{\sigma_{\xi,lam}} + \frac{\mu_{tur}}{\sigma_{\xi,tur}}\right]\frac{\partial\widetilde{\xi}}{\partial x_k}\right\} \tag{4.4}$$

and

$$\frac{\partial\overline{\rho}\widetilde{\xi}^{"2}}{\partial t} + \frac{\partial}{\partial x_k}(\overline{\rho}\widetilde{u}_k\widetilde{\xi}^{"2}) = \frac{\partial}{\partial x_k}\left\{\left[\frac{\mu_{lam}}{\sigma_{\xi,lam}} + \frac{\mu_{tur}}{\sigma_{\xi,tur}}\right]\frac{\partial\widetilde{\xi}^{"2}}{\partial x_k}\right\} +$$

$$c_{g1}\mu_{tur}\left(\frac{\partial\widetilde{\xi}}{\partial x_k}\right)^2 - c_{g2}\overline{\rho}\left(\frac{\widetilde{\varepsilon}}{\widetilde{k}}\right)\widetilde{\xi}^{"2} \tag{4.5}$$

where $\bar{\rho}$ is the mean density, $\tilde{u}_k$ and $\tilde{\xi}^{"2}$ are the Favre-averaged components of the velocity in the x_k-direction and the mixture fraction fluctuation around its mean value, respectively, μ_{lam} and μ_{tur} are laminar and turbulent viscosities, and $\sigma_{\xi,,lam}$ and $\sigma_{\xi,,tur}$ are the effective Prandtl/Schmidt numbers, respectively. The empirical constants, c_{g1} and c_{g2}, have values of 2.8 and 2.0, respectively. The parameters $\tilde{k}$ and $\tilde{\varepsilon}$ are the Favre-averaged turbulent kinetic energy and viscous dissipation terms, given by their balance equations

$$\bar{\rho}\tilde{u}_k \frac{\partial k}{\partial x_k} = \frac{\partial}{\partial x_k}\left\{\left(\mu + \frac{\mu_{tur}}{\sigma_{k,tur}}\right)\frac{\partial k}{\partial x_k}\right\} - \bar{\rho}\widetilde{u_i}^{"}\widetilde{u_k}^{"}\frac{\partial \tilde{u}_i}{\partial x_i} - \frac{\mu_{tur}}{\tilde{\rho}^2}\frac{\partial \bar{\rho}}{\partial x_i}\frac{\partial \bar{\rho}}{\partial x_i} - \bar{\rho}\varepsilon \quad (4.6)$$

and

$$\bar{\rho}\tilde{u}_k \frac{\partial \varepsilon}{\partial x_k} = \frac{\partial}{\partial x_k}\left\{\left(\mu + \frac{\mu_{tur}}{\sigma_{\varepsilon,tur}}\right)\frac{\partial \varepsilon}{\partial x_k}\right\} -$$

$$c_{\varepsilon 1}\frac{\varepsilon}{k}\left(\bar{\rho}\widetilde{u_i}''\widetilde{u_k}''\frac{\partial \tilde{u}_i}{\partial x_k} + \frac{\mu_{tur}}{\tilde{\rho}^2}\frac{\partial \bar{\rho}}{\partial x_i}\frac{\partial \bar{\rho}}{\partial x_i}\right) - c_{\varepsilon 2}\bar{\rho}\frac{\varepsilon^2}{k} \quad (4.7)$$

where u''_i and u''_k are fluctuating parts of the velocities in the x_i and x_k – directions, and $\sigma_{k,,lam}$ and $\sigma_{\varepsilon,,tur}$ are the effective Prandtl/Schmidt numbers for k and ε, respectively.

To be accessible for CFD (SOFIE) the flamelet lookup tables are pre-computed from the instantaneous state relationships by integrating for each property throughout the mixture fraction and mixture fraction variance space. The mixture fraction mean has been discretised in 101 divisions and the mixture fraction variance in 51 divisions. The minimum and maximum values of mixture fraction variance of 0.001 and 0.1, respectively, have been employed. A block scheme of the current version of the flamelet model for use in SOFIE is shown in Figure 4.1. As the turbulence intensity of fires in atmospheric conditions is relatively low compared with other combustion processes such as internal combustion engines, only low strain rates are taken into account. The flamelets are, however, calculated up to extinction values of strain rate. When simulating fire with very high turbulent intensity, the flamelets for higher strain rate should be chosen into calculations.

For every vitiation fraction 30 different flamelet sets, each with their own radiation heat loss level (from zero to 30% heat loss) incremented by 1 % for every individual species, are included in the library. This model is still to be run with a single value for vitiation in the whole calculation domain at a given time, and not with an individual vitiation for each cell. Such a method would require an additional dimension in the lookup table, which would need much more computer storage and much greater running times.

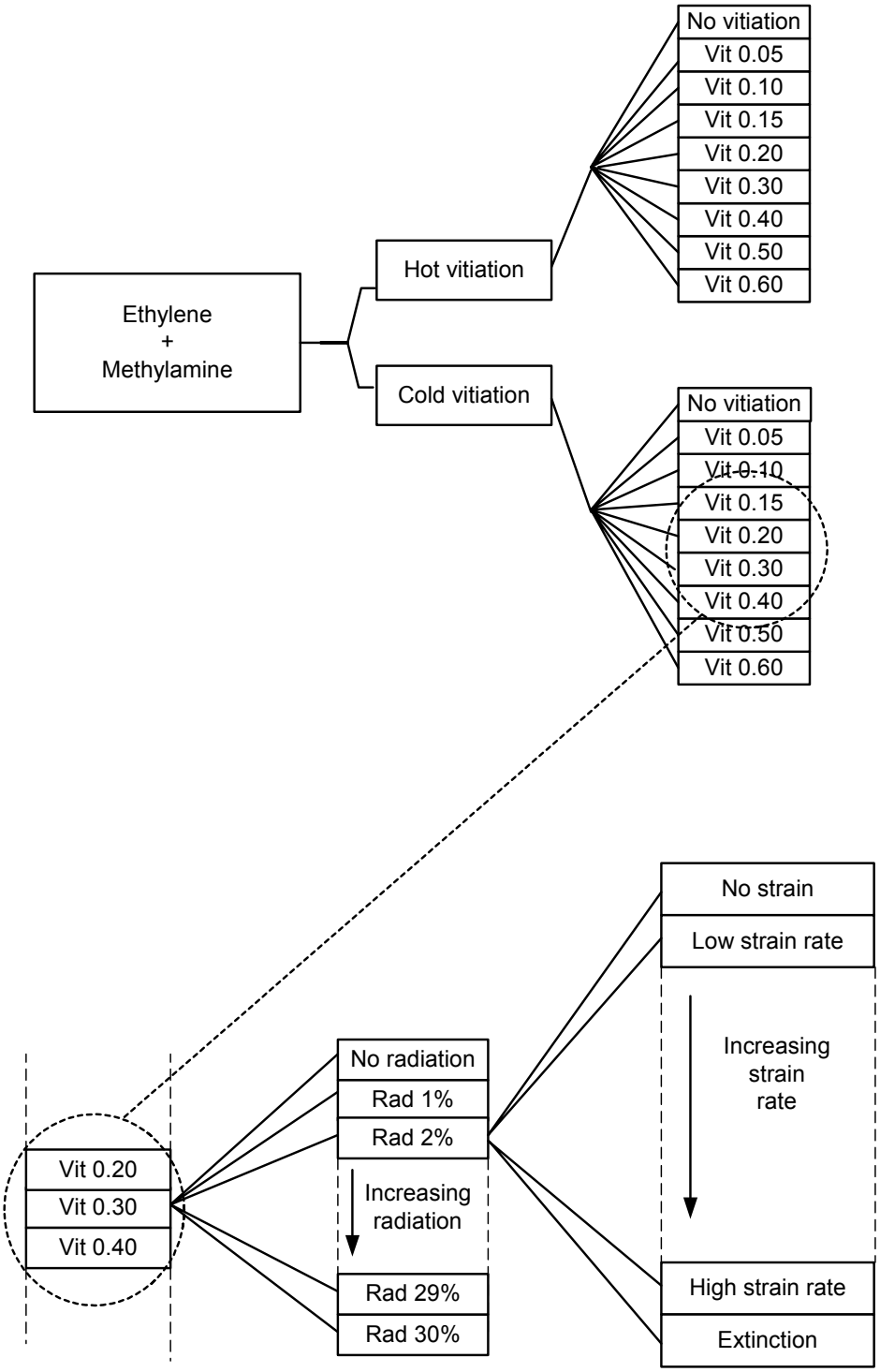

Figure 4.1 Flamelet library structure for vitiated and non-vitiated air used in SOFIE. For each vitiation fraction there are 30 different sets of flamelets for each radiation increment and for each radiation level there are 30 individual sets of flamelets for varying strain rate.

5 Full scale validation data and design fires

5.1 Fire tests used for initial validation of the model

The flamelet model has been validated against laboratory measurements performed previously at SP fire laboratory [19]. The fire tests were conducted in a room with dimensions according to the ISO 9705 Room corner test. The room has one door opening of size 0.8 m x 2.0 m (see Figure 5.1). Changing the size of the door opening varied the ventilation rate to the fire in the tests. For post-flashover (ventilation controlled) compartment fires the inflow rate of air is given by [20]

$$\dot{m} \approx 0.5 \cdot A \cdot \sqrt{H} \qquad (5.1)$$

where A is the area of the opening in m^2 and H is the height of the opening in m.

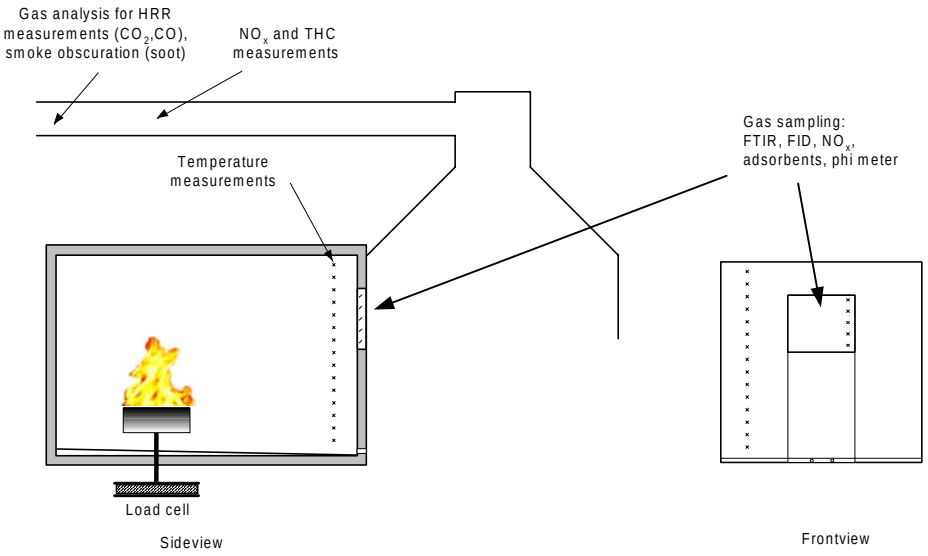

Figure 5.1. The test arrangement used in laboratory measurements [19]. The size of the opening was varied between tests to adjust the ventilation rate. The fire source was placed on the floor in the room centreline at a distance 1/3 of the room length from the back wall. A fuel pan of size 1.44 m^2 (1.2m x 1.2m) was loaded with nylon. HCN was measured with FTIR in the door opening.

In the fire tests used for validation purposes here, nylon was used as a fuel. To reduce the door opening area the lower part of the opening was blocked. Tests with opening heights of 0.89 m and 0.56 m were used for validation. The test with an opening height of 0.89 m gave a steady state fuel mass flow of 20 g/s corresponding to 500 kW after the initial fire growth period. The fire stayed rather constant at this burning level until the end of the experiment where the burning rate raised somewhat and the test was manually extinguished. The test with an opening height of 0.56 m yielded, as expected, initially a lower mass flow rate of fuel, about 15 g/s, corresponding to 350 kW RHR. This test had however a shorter steady-state period, after where the burning rate enhanced to reach a

RHR above 500 kW. This test reached flashover conditions before it was manually extinguished.

Gas temperatures were measured using 0.5 mm type K thermocouples inside the room and in the door opening. Inside the room the thermocouples were placed on a vertical thermocouple tree 30 cm from the two walls in the front left corner. In the opening the thermocouples were placed in a smaller vertical tree 10 cm from the right hand side of the opening (see Fig. 5.1) [19].

The probe for the measurement of gas species (FTIR was used for the measurement of HCN [21]) and the probe for the measurement of the PHI-value (the PHI-value is a measure of the global equivalence ratio [20]) were placed diagonally from the top left (seen from outside) corner to the middle of the other side of the opening and varied in length depending on the size of the opening. The suction end of the probes was in the top corner. This arrangement was supposed to achieve representative sampling over the opening because of larger suction in the part of the opening with the lowest density of the smoke gases. The probes were made of stainless steel tubing with 6 mm inner diameter and had holes with a diameter of 3 mm, at distances of 10 cm in between, the number of holes depending on the length of the probe.

5.2 Description of the design fires

The nitrogen content of nylon is close to that of the computer model fuel mixture 1 (ethylene/methylamine ratio 3). However, the mass loss rate at a given heat release rate is about 30% less for the mixture 1 fuel compared to nylon (i.e. the model fuel has a higher effective heat of combustion). As the level of HRR decides the demand of the oxygen in combustion, the same HRR, and thus the same degree of vitiation, as in the tests was assumed for the simulations. The concentrations of certain products of combustion, such as HCN and CO, can thus be lower, provided that the bounding of the nitrogen in the fuel has no major influence, see section 7.6. This needs to be discussed further together with other aspects concerning the flame temperature in nylon combustion compared to the chosen fuel in the calculations. However, for a real fuel, such as nylon, the mass loss is expected to be larger compared to the idealised situation in the model, because all the fuel released in a real fire does not take part in the combustion in certain situations.

For the scenario with an opening height of 0.89 m, the rate of heat release was assumed to grow as $\dot{Q} = \alpha t^2$, with α = 8.68 W/s^2 up to value of 500 kW during the pre-burn time period (first four minutes), after which the RHR was held constant at that level. This t^2-approximation was chosen to help the computation of the initial flow field. Similarly for the scenario with an opening height of 0.56 m, the RHR was assumed to grow as t^2 with time up to 350 kW.

In the computer model a fire source was placed in the room with area and position corresponding to the fire tests. The simulated walls were assumed to consist of lightweight concrete. The upper half of the walls and the ceiling was covered with a 5 cm layer of high-density mineral wool to avoid damage to the walls in real tests. To simulate the same physical environment as closely as possible the mineral wool covering was modelled similarly in the computer model. Figure A4 in Appedix A, shows the computer model of the room with an opening height of 0.89 m.

An open atmosphere in the front of the opening was included in the simulations. The calculation domain was extended outside the room about the length of the room and twice the height of the room. The outermost face of the atmosphere opposite to the door was assigned a static pressure boundary, through which the air freely passes in and out of the calculation domain. To save computing time, the region above the ceiling of the room was treated as an inactive blockage, where no transport equations were solved.

6 CFD simulations

The calculation domain was divided in 233 100 small control volumes (42 x 75 x 74 in *x*, *y* and *z* directions, respectively). This corresponds to an average cell size of about 10 cm. The space was divided finest in the combustion region, where the largest gradients in field parameters are expected. In the fire plume and a vicinity of it, a typical cell size between 2 and 5 cm was used. Especially, in vertical direction (*y*-coordinate) the space was divided finely, to be able to resolve the chemistry in the plume flow. In the other regions inside the room a typical cell size of 10 cm, and outside the room 15 to 25 cm, were used.

The convergence of the solution was controlled keeping all solved variable's residuals (normalised) as low as possible, usually below 0.001. The under-relaxation parameters for momentum were set to 0.12 at the beginning of the simulation and were reduced further to about the half value of that later in simulation to avoid the oscillating behaviour in solution.

The simulations were made using the transient mode of SOFIE. The length of the time step was chosen, depending the actual situation occurring during the fire history. In the beginning and during most of the simulation time a time step of one second was used. Approaching the under-ventilated situation the time step was shortened. In the most under-ventilated situation, i.e. when using the smallest opening, as short as 0.25 s time step was necessary to establish a converged solution.

Although the flamelet lookup tables for use in SOFIE are made for varying radiation, the model can be used in several different ways: as adiabatic flamelets, non-adiabatic flamelets with fixed radiation and non-adiabatic flamelets with varying radiation. In this work the flamelet sets were pre-calculated with up to 30% radiation losses incremented by 1%, i.e. all species, temperature, density and enthalpy have their own columns for each radiation level.

Using the adiabatic mode, only the first columns (with no radiation losses) of each flamelet set are taken into account. Using the non-adiabatic flamelets with varied radiation one has to choose either of the three sub-commands: upper, lower, or interpolated bounding flamelet. In the first two cases SOFIE then chooses the nearest upper or lower radiation columns from the flamelet tables. Using the non-adiabatic flamelet option with interpolated radiation SOFIE selects automatically the right radiation levels through interpolation between adjacent levels in the flamelet tables.

All the simulations presented in this report were made using the non-adiabatic flamelet mode with interpolated radiation.

It is however worth to mention that the radiation options in SOFIE can also be used to manipulate the radiation heat losses from the flamelets by specifying the adiabatic set other than the first column in the lookup tables. This is physically not exactly correct because the thermo-chemical parameters for the appropriate flamelet sets do not match those calculated in adiabatic conditions. However, in some cases this is useful, when one wants to attenuate or strengthen the radiation from flames.

The discrete transfer radiation model (DTRM) assuming 16 rays (default value) was used in the simulations. No soot model was used, and hence the radiation from soot was not included. It was not possible to use a lager number of rays in these simulations, because

the chemical model reserved so much computer memory, that the computations could not have been performed in a reasonable time.

6.1 Comparison with measurements

The simulations were run with non-vitiated and vitiated flamelet options. In vitiated cases the vitiation fraction was manually switched to higher levels when the oxygen concentration in the entrainment region to the flame was reduced to the level corresponding with that vitiation. The following cases were run with fuel mixture 1 (corresponding to approximately the same nitrogen contents as nylon):

Case 1: No vitiation, opening height 0.89 m
Case 2: Vitiation, opening height 0.89 m
Case 3: Vitiation, opening height 0.56 m

In vitiated cases the degree of vitiation was manually changed based on the oxygen contents of the air entrained to the fire. The first 160 s in case 2 were run as non-vitiated. At 160 s the vitiation fraction 0.05 was chosen. At 180 s the vitiation fraction was increased to 0.15, at 200 s to 0.20 and after 240 s the vitiation fraction was held at 0.30. In case 3 the vitiation fraction was increased more rapidly, so that the vitiation fraction of 0.30 was reached at 180 s. The actual vitiation increased to near the 0.40 level after 240 s, but the low oxygen contents (12.6 %) in the air using this vitiation level made that solution non-convergent. It seemed that the low oxygen concentration was not able to sustain combustion in the model. Thus, the vitiation fraction 0.30 was used during the rest of the simulation.

6.1.1 Gas temperatures

Tables 6.1 through 6.3 summarise the calculated and measured gas temperatures for case 1 through 3. In all cases T_1, T_2 and T_3 are temperatures at heights 2 m, 1.4 m, and 0.95m in the front left corner of the room, respectively (selected temperature points from the corner thermocouple tree, see previous chapter and Fig. 5.1). $T_{opening}$ is the temperature of out-flowing gas from the door opening, 10 cm below the soffit for cases 1 and 2, and 8 cm below the soffit for case 3. The correction calculations of the thermocouple temperatures were made, which showed no noticeable errors (maximum error approximately 20 K) in recorded temperatures located both inside the room and in the opening.

The results are compared after the so-called pre-burn period, when the heat release rate (HRR) has been stabilised at a constant level. In the computer simulations that pre-burn time was four minutes during which the HRR increased as t^2 (see previous chapter). In the tests the pre-burn time was longer and the HRR history more undefined due to the ignition behaviour of the fuel.

In the non-vitiated case (Table 6.1) the gas temperatures in the corner location are generally 10-20 % lower than the measured temperatures. In the vitiated case (Table 6.2) these temperatures are closer to the measured values, discrepancy about 5 -15 %. At the opening the difference between the measured and calculated temperature are negligible; less than 2 % in both vitiated and non-vitiated cases.

Table 6.1. Calculated values of gas temperatures (°C) compared with measured values. Case 1: opening height 0.89 m. Non-vitiated flamelet option used.

Time [min] after pre-burn	Calculated				Measured			
	T_1	T_2	T_3	$T_{opening}$	T_1	T_2	T_3	$T_{opening}$
0	570	536	459	551	637	600	509	532
1	578	541	468	553	695	649	550	557
2	582	547	474	564	716	670	575	567

Table 6.2 Calculated values of gas temperatures (°C) compared with measured values. Case 2: opening height 0.89 m. Vitiated flamelet option used.

Time [min] after pre-burn	Calculated				Measured			
	T_1	T_2	T_3	$T_{opening}$	T_1	T_2	T_3	$T_{opening}$
0	601	562	481	537	637	600	509	532
1	621	582	501	555	695	649	550	557
2	622	582	501	558	716	670	575	567

The scenario with smaller opening (Table 6.3) was simulated with vitiation only. Once again the calculated temperatures inside the room are lower than those measured. The temperature discrepancy is of the same order as in the vitiated case for the larger opening (Case 2). The simulated temperatures at the opening agree well with the measured temperatures, although the difference is slightly larger than in scenario with larger opening.

The temperature fields at room centreline for the three cases are shown in Appendix A

Table 6.3 Calculated values of gas temperatures (°C) compared with measured values. Case 3: opening height 0.56 m. Vitiated flamelet option used.

Time [min] after pre-burn	Calculated				Measured			
	T_1	T_2	T_3	$T_{opening}$	T_1	T_2	T_3	$T_{opening}$
0	575	537	467	518	610	576	519	535
1	590	545	469	525	626	593	535	536
2	605	549	467	525	667	631	563	559

6.1.2 Species concentrations

The main species concentrations are summarised in tables 6.4 – 6.6. Both calculated HCN and CO concentrations are much lower than measured values when the non-vitiated flamelet option is used (Table 6.4). This indicates that in room fires the vitiated scenario is the real one, because the fire gases are recycled back to fire in reality. In a vitiated case

(Table 6.5) the HCN levels are about 7-8 times higher than in the non-vitiated case, even though they are lower compared to measured values. The calculated CO concentrations in the non-vitiated case are about a half of the measured concentrations. In the vitiated case the calculated CO concentrations are, on the other hand, higher than the measured values, especially later in the experiment.

The CO_2 concentrations are generally higher than the measured values, calculated using the non-vitiated option, and lower using vitiation. This indicates that the combustion is more complete with a non-vitiated case than with a vitiated case. The real fire is vitiated and hence the combustion is less complete. Hence, the vitiation option gives more CO and HCN and generally less CO_2 than the non-vitiated option. Generally, of these two options the best agreement with measurement is the vitiated option, see table 6.5.

Table 6.4 Calculated species concentrations and global equivalence ratio in the opening compared with measured values. Case 1: opening height 0.89 m. Non-vitiated flamelet option used.

Time [min] after pre-burn	Calculated			Measured			
	HCN [ppm]	CO [ppm]	CO_2 [%]	HCN [ppm]	CO [ppm]	CO_2 [%]	Φ
0	2.2	193	4.89	30.2	293	4.30	0.55
1	3.3	214	5.30	35.8	448	4.16	0.55
2	3.4	219	5.39	34.6	456	4.23	0.55

Table 6.5 Calculated species concentrations and global equivalence ratio in the opening compared with measured values. Case 2: opening height 0.89 m. Vitiated flamelet option used.

Time [min] after pre-burn	Calculated			Measured			
	HCN [ppm]	CO [ppm]	CO_2 [%]	HCN [ppm]	CO [ppm]	CO_2 [%]	Φ
0	15.4	279	3.42	30.2	293	4.30	0.55
1	23.3	629	4.45	35.8	448	4.16	0.55
2	27.1	736	5.50	34.6	456	4.23	0.55

When reducing the opening size the measured concentrations of HCN are increased by a factor 6-10 in the initial steady-state period (Table 6.6). This trend is also seen with the calculated results, but the increase is stronger, generally more than a factor 10. The vitiation of the air in the room increases faster in the case with the smaller opening which is reflected in the higher Phi-values measured in Case 3. The higher vitiation lowers the gas temperature and thus influences the gas chemistry and causes a significantly higher production of HCN (see e.g. Figure B1-c). Also the CO concentrations are higher in the scenario with smaller opening. In particular the calculated values increase strongly, by a factor 5. The measured CO concentrations increase by a factor of about 2 when the opening size is reduced.

Table 6.6 Calculated species concentrations and global equivalence ratio in the opening compared with measured values. Case 3: opening height 0.56 m. Vitiated flamelet option used.

Time [min] after pre-burn	Calculated			Measured			
	HCN [ppm]	CO [ppm]	CO_2 [%]	HCN [ppm]	CO [ppm]	CO_2 [%]	Φ
0	246	2202	8.20	291	1018	9.02	0.70
1	384	3582	8.31	220	791	8.63	0.70
2	431	3582	8.41	218	784	8.37	0.75

Species concentration fields at the room centreline are shown in Appendix A

7 Representation of the chemical kinetics

The complete methylamine oxidation mechanism used in this study consists of 350 elementary reaction steps according to Kantak *et al* [22], including the following pathways:

- H-atom abstraction
- C-N bond scission
- Formation of HCN and NH_3
- Recombination reactions of species H_2CN and CH_3NH

The structure formula of methylamine is schematically shown in Figure 7.1.

Pathways leading to formation of HCN are usually subsequent H-abstractions starting from CH_3NH_2.

$$CH_3NH_2 \rightarrow \text{intermediate} \rightarrow \text{smaller intermediate} \rightarrow HCN \quad \text{(R1)}$$

The products after C-N bond scission reactions play usually a minor roll in formation of HCN. However, some recombination reactions connecting carbon and nitrogen again are possible in some circumstances.

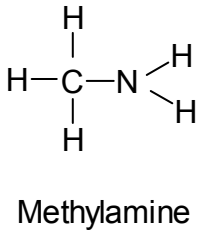

Methylamine

Figure 7.1 Structure formula of methylamine.

7.1 H-atom abstraction

There are two possibilities for the first H-atom abstraction from a CH_3NH_2 molecule. It can occur either at the C-atom centre or at the N-atom centre as:

$$CH_3NH_2 + X \rightarrow CH_2NH_2 + XH \quad \text{(R2)}$$

and

$$CH_3NH_2 + X \rightarrow CH_3NH + XH, \quad \text{(R3)}$$

where X is an arbitrary radical. H-atom abstraction by O-atoms (i.e. X = O) at C- and N-atom centres, respectively, are:

$$CH_3NH_2 + O \rightarrow CH_2NH_2 + OH \quad \text{(R4)}$$
$$CH_3NH_2 + O \rightarrow CH_3NH + OH \quad \text{(R5)}$$

Similarly H-atom abstraction by OH radical to form H_2O occur with reactions:

$$CH_3NH_2 + OH \rightarrow CH_2NH_2 + H_2O \quad (R6)$$
$$CH_3NH_2 + OH \rightarrow CH_3NH + H_2O \quad (R7)$$

Corresponding reactions with H radical to form H_2 are:

$$CH_3NH_2 + H \rightarrow CH_2NH_2 + H_2 \quad (R8)$$
$$CH_3NH_2 + H \rightarrow CH_3NH + H_2 \quad (R9)$$

There are differences in opinion between investigators whether the C-H or N-H branching is the most probable. According to some speculations C-H to N-H ratio is about 10 at 1600 K [22], but the experimental data to support these speculations is lacking.

Based on the study of Kantak *et al* [22] the overall effect of C-H/N-H branching ratio is about 60/40. According to their investigation the preference of C-H and N-H abstraction could be close to 50/50, because the bond energies for both bound types differ by less than 5%, and the energies of CH_2NH_2 and CH_3NH are of the same order. Therefore, assuming further that the CH_3NH_2 attacked by the collider atom similarly at both N- or C-centres, the H-atom availability of 3/2 at C- and N-centres of the CH_3NH_2 molecule recommends to use of a 60/40 branching ratio.

7.2 C-N bond scission

The C-N bond scission of methylamine occurs via third body reaction, which leads to formation of methyl radical and amine:

$$CH_3NH_2 + M \rightarrow CH_3 + NH_2 + M \quad (R10)$$

and by reaction with H radical forming the methyl radical and ammonia:

$$CH_3NH_2 + H \rightarrow CH_3 + NH_3 \quad (R11)$$

Also the intermediate species CH_3NH and CH_2NH_2 formed as results from the first H abstraction undergo C-N bond scission by O, OH, H and O_2 radical attacks. The N containing parts of the dissociation products are NH, NH_2 and HNO. The CH_3NH reactions are:

$$CH_3NH + O \rightarrow CH_3O + NH \quad (R12)$$
$$CH_3NH + OH \rightarrow CH_4 + HNO \quad (R13)$$
$$CH_3NH + H \rightarrow CH_3 + NH_2 \quad (R14)$$
$$CH_3NH + O_2 \rightarrow CH_3O + HNO \quad (R15)$$

The CH_2NH_2 is dissociated with C-N bond scission similarly:

$$CH_2NH_2 + O \rightarrow CH_3O + NH \quad (R16)$$
$$CH_2NH_2 + OH \rightarrow CH_4 + HNO \quad (R17)$$
$$CH_2NH_2 + H \rightarrow CH_3 + NH_2 \quad (R18)$$
$$CH_2NH_2 + O_2 \rightarrow CH_3O + HNO \quad (R19)$$

Species CH_3NH and CH_2NH_2 can alternatively react first with H or any other radical in a H-abstraction reaction resulting H_2CNH, which then dissociates similarly by C-N bond scission to form formaldehyde, NH and NH_2:

$$H_2CNH + O \rightarrow CH_2O + NH \quad \text{(R20)}$$
$$H_2CNH + OH \rightarrow CH_2O + NH_2 \quad \text{(R21)}$$

Carbon containing products of C-N scission generally will oxidise further to the stable products CO and CO_2, while nitrogen-containing products will oxidise to NOx, N_2O and N_2. The intermediate H_2CNH seems to be a potential source of HCN.

7.3 Formation of HCN

The most probable pathways leading to the formation of HCN are subsequent H-abstraction reactions starting from fuel. After breaking of the C-N bond the component containing N oxidises further to NOx or stable molecules, N_2O and N_2. A small fraction of N-containing component may recombine with C-containing components to form species with C-N bonds.

Because, HCN is a result of series of H-abstraction reactions that CH_3NH_2 intermediates undergo during the fuel pyrolysis process, the main part of the HCN is formed in the combustion zone. As a result from the second H-abstraction from the CH_3NH_2 molecule an important HCN precursor, H_2CNH, is formed via intermediate species CH_2NH_2 (reactions R4, R6 and R8) and CH_3NH (reactions R5, R7 and R9):

$$CH_2NH_2 + X \rightarrow H_2CNH + XH \quad \text{(R22)}$$

and

$$CH_3NH + X \rightarrow H_2CNH + XH \quad \text{(R23)}$$

The H_2CNH then decomposes via two main paths to HCN; either via H_2CN or via HCNH:

$$H_2CNH \begin{cases} \nearrow \; HCNH \; \searrow \\ \searrow \; H_2CN \; \nearrow \end{cases} HCN \quad \text{(R24, R25) / (R26, R27)}$$

Which of the two paths that are favoured to form HCN depends on the combustion environment. According to Hjuler *et al* conditions [23] the HCN was formed via $H_2CN \rightarrow$ HCN by a factor 5 more than via HCNH $\rightarrow$ HCN. Under Basevich's conditions [24] HCN was formed mainly via HCNH $\rightarrow$ HCN (93-95%). Whatever the path is, the study presented by Kantak *et al* shows that the most of HCN is formed via H_2CNH.

The magnitudes of HCN formation under Both Hjuler's and Basevich's conditions are valid for the same temperature, 1160 K. The Basevich's conditions were at low pressure (0.01atm), at equivalence ratios between 0.23 and 1.7, and 2.5 ms residence time. The Hjuler's conditions were those similar of the post-flame conditions in industrial incinerators, i.e. near atmospheric conditions.

This study shows that the major part of the HCN is formed by decomposition of fuel through a series of H-atom abstraction. This indicates that the most of the HCN is formed in the pyrolysis process. This effect was also seen in the results from CFD simulations. A high concentration of HCN was seen within a thin region just above the fuel bed, even at well-ventilated conditions (see Figure A1-a). Under more vitiated conditions the HCN concentration becomes higher and HCN is spreading far away from the fire (Figure A3-a).

7.4 Main reaction paths to HCN formation

The possible reaction pathways from fuel to HCN are enormous in reality. To construct the main pathway map several simplifications must be made. The authors in ref [22] have performed integrated reaction-path analysis to construct a molecular roadway maps for oxidation of CH_3NH_2 at 1160 K in several conditions. The pathway map is shown in Figure 7.1.

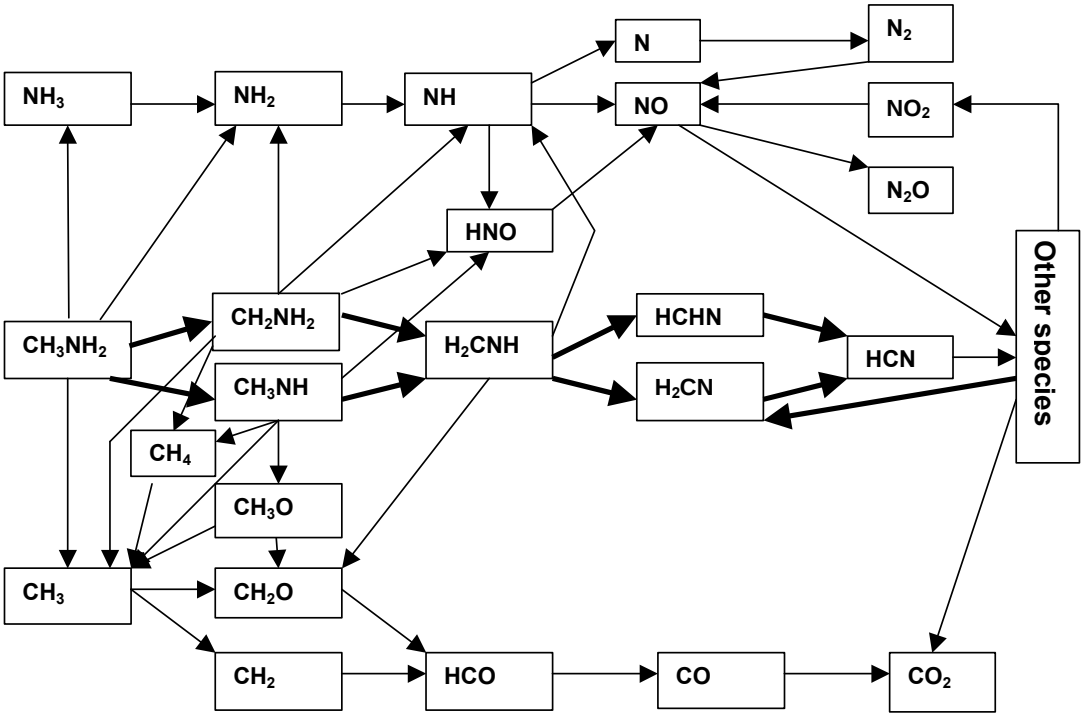

Figure 7.1. The integrated main reaction paths for methylamine at fire temperatures [22]. The species that contain a C-N bond follow the pathway marked by thick arrows. A series of H-atom abstraction reactions lead to formation of HCN via this pathway. The C-N bond scission reactions lead to formation of carbon (upper paths) and nitrogen (lower paths) containing species.

The reaction paths are similar in a wide range of equivalence ratios but the relative magnitudes differ with the equivalence ratio (and pressure and temperature). At Basevich's conditions, T = 1160 K, and p = 0.01 atm the ratios of H-abstraction to C-N scission are 86/14, 89/11 and 90/10 for ϕ = 0.23, 1.0 and 1.7, respectively. This means that the H-abstractions dominate the reaction paths, even though the C-N bond breaking

is quite large. Especially, the initial C-N bond scission reaction is large under these conditions. The C-N bond scission decreases in magnitude with increasing equivalence ratio. This means that pathways coloured by blue in the Figure 7.1 are more dominating in the rich mixtures, and hence the larger amount of HCN is formed.

The conditions of Hjuler *et al* [23] represent conditions corresponding to post-flame regions of an industrial incinerator. These conditions represent better the conditions that occur in fires. According to their study the initial C-N bond scission in destruction of CH_3NH_2 is very low, about 2 % of the total destruction rate, and the remaining 98 % is due to H-atom abstraction. This means that paths leading to formation of HCN dominate, see Figure 7.1. The interesting is the difference in the magnitudes of the final part of the pathway ending with HCN, i.e. the last H-abstraction (in the 'blue' pathway in Figure 7.1) from intermediate species HCNH and H_2CN. At low pressure the HCN was formed mainly via HCNH $\rightarrow$ HCN rather than via $H_2CN \rightarrow$ HCN. At atmospheric post-flame conditions the latter path was favoured by factor 5 over the former path.

When looking the pathway map in Figure 7.1, it is obvious that most of HCN is formed from molecules, or molecule fragments that already contain a C-N bond. Other ways, except than decomposition of Nitrogen-Hydrogen containing fuel to formation of HCN, are recombination of carbon- and nitrogen containing radicals, in which new C-N bonds are build. The resultant species may pass trough a series of H abstraction reactions ending with HCN. At sufficiently high temperatures the nitrogen, which is naturally in air, may react with carbon containing radicals, CH, and CH_2 directly forming HCN [22]

$$CH + N_2 \rightarrow HCN + N \quad \text{(R28)}$$
$$CH_2 + N_2 \rightarrow HCN + NH \quad \text{(R29)}$$
$$CH_2 + N \rightarrow HCN + H \quad \text{(R30)}$$

Similarly HCN may be formed from NO via reaction with carbon containing radicals or with CH_3 :

$$CH + NO \rightarrow HCN + O \quad \text{(R31)}$$
$$CH_2 + NO \rightarrow HCNO + H \quad \text{(R32)}$$
$$HCNO + H \rightarrow HCN + OH \quad \text{(R33)}$$
$$CH_3 + NO \rightarrow HCN + H_2O \quad \text{(R34)}$$

The reactions R28 through R34 may occur also in combustion of non-nitrogen containing fuels. Formation of HCN from ambient nitrogen requires higher temperature compared to HCN formation from fuel-based nitrogen. The reactions R28 through R34 occur in the reaction zone in the flame sheet. The pathways of these reactions are not shown in Figure 7.1, because they are assumed to give minor contribution to total HCN formation. The less important pathways are omitted or are included in the box 'Other species'.

However, the major part of the fuels in our study was ethylene (C_2H_4), which may increase the important of the HCN formation via other paths than from the fuel at higher temperatures. The reactions R28 through R34 may also play larger roll in fully developed room fires, just after flashover, when the temperature is high and the oxygen concentration is rapidly lowered due to increased heat release rate, resulting in large amounts of C-containing radicals in the gas layer.

The CFD simulations showed that when the ventilation rate was lowered, the formation of HCN was increased. When using the vitiated flamelets (which better describes the environment in the room tests) in the calculations, the HCN concentration was increased, which indicates that at fuel-rich and vitiated conditions the oxidation of the species in the

two pathways for the carbon- (the red pathways in the Figure 7.1) and the nitrogen-containing (the green pathways) species is lowered. This means that the reactions leading to HCN formation increase relatively (the blue pathways).

7.5 Destruction of HCN

Later in the flow stream, depending on the concentration of oxygen, and certain radicals (as H, O and OH), HCN may be oxidised to eventually form NOx. One of the reasons for higher concentrations of HCN in under-ventilated conditions might be that the rate of oxidation of HCN to NOx is reduced (or interrupted), so that more HCN is left in the gas stream. The destruction of HCN was described by the following reactions (R 35 – R41):

$OH + HCN \rightarrow HOCN + H$ (R35)
$OH + HCN \rightarrow HNCO + OH$ (R36)
$OH + HCN \rightarrow NH_2 + CO$ (R37)
$HCN + O \rightarrow NCO + H$ (R38)
$HCN + O \rightarrow NH + CO$ (R39)
$HCN + O \rightarrow CN + OH$ (R40)
$CN + HCN \rightarrow C_2N_2 + H$ (R41)

No analysis of the relative importance of these destruction reactions has been made in this work, it is however obvious that the oxygen concentration is important in the destruction process.

7.6 Some aspects of nylon combustion

The interest in studies of the nitrogen chemistry in combustion has arisen from the need to understand the mechanisms behind NOx formation. Earlier research by Fenimore [25] indicated that the conversion of organic nitrogen compounds to NOx was nearly independent of the parent molecule, and that local combustion conditions and the initial concentration of the nitrogen species were the dominant factors. Fenimore further speculated that an intermediate product was formed that could react to either NO or N_2 depending on the combustion conditions. Bowman [26] later proposed that for simple nitrogen containing fuels, a reasonable prediction of NOx formation could be achieved by using a global reaction step of fuel-nitrogen → HCN combined with the detailed HCN chemistry. Regarding the conversion of a nitrogen-containing fuel to gaseous pyrolysis products, it can further be found in Glassman [27] that HCN is one of the domination intermediates in the conversion of fuel nitrogen to NO.

In this work a kinetic scheme of the conversion of the fuel methylamine to combustion products has been applied. The detailed reaction mechanism for the C-N intermediates to form HCN is included. The simulations discussed in this report was however of fire tests with nylon as a fuel. To quantitatively compare the results of the experiments with those of the simulation one has to make the presumption that the pyrolysis chemistry of nylon gives the same types and proportions of breakdown products as those described by the reaction mechanism for methylamine. Such a presumption would perhaps not be entirely true, but based on the more qualitative knowledge discussed above that “the conversion of organic nitrogen compounds to NOx (where HCN is the major intermediate product) is nearly independent of the parent molecule” semi-quantitatively results with some significance would be attainable with the present approach.

The results (see Section 6) of these first simulations with methylamine as a model fuel representing an arbitrary nitrogen containing fuel (nylon in this case) indicate however that our approach has some success.

With more knowledge of the pyrolysis chemistry of nylon one would be able to make a better assessment of the justification of using methylamine as a model fuel in this case. Studying the structure of the polymer chain of Nylon-6,6 (Figure 7.2) one can foresee that during thermal decomposition the initial products would be a mixture of low-molecular-weight fragments, some containing nitrogen.

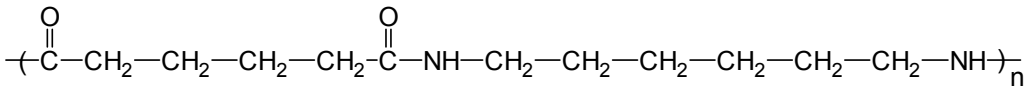

Figure 7.2 Structure formula of nylon-6,6.

It has been shown that the thermal decomposition of various nylons begin with a primary scission of an –NH·CH_2– bond to form amides and is followed by a complex series of secondary reactions [28]. Nitriles can, e.g., be subsequently formed from these amides through high temperature dehydration [29]. Other researchers [30] has postulated that in the pyrolysis of nylon-6,6, substituted cyclopentanone groups are formed by NH-CO bond scission and ring closure. This last decomposition route would thus lead to the formation of NH-R fragments that would fit in the reaction scheme of methylamine (where $HNCH_2$ is important). One can conclude that the thermal decomposition and subsequent reaction chemistry of nylon is complex and it has not been possible to fully investigate it in this project.

8 Discussion and Conclusion

A mathematical simulation model of the production of HCN from fires based on chemical kinetics has, to the knowledge of the authors of this report, not been presented before. It is however well known that HCN can be produced in hazardous amount from fires with nitrogen-containing materials, especially under vitiated combustion conditions, such that occur in room fires.

Actually, very little work has been reported in the literature concerning the calculation of fires in vitiated air. The flamelet models have, in the last 10 years, been more commonly applied in CFD models. However, most models use flamelets calculated in pure air. In most situations that occur in a room fire, this does not represent the right picture for the chemical species calculation. Due to ventilation restrictions the combustion products vitiate the air in the compartment. As fires naturally need air for the combustion, the entrained air in a closed room or a room with small openings is vitiated.

The chemistry of combustion, especially in oxygen poor conditions is a very complicated process. The vitiation reduces the chemical reaction rates and increases the formation of products of incomplete combustion, such as CO. If the fuel contains nitrogen, HCN is also formed, which is demonstrated in the present work.

The results from the simulations with the nitrogen-containing model-fuel presented in this report show that that the present flamelet model is able to semi-quantitatively predict the production of HCN in a room fire with nylon as the fuel. Both the production during well ventilated, and the increased production during under-ventilated conditions, was captured by the model. The presented simulations with the model should however be regarded as an initial test only of the models capability to simulate the gas-phase chemistry of fires with an arbitrary nitrogen-containing fuel.

There are some obvious weaknesses of the present application of the model. The model-fuel is based on the chemistry of gas-phase methylamine mixed with ethylene, and does not describe the pyrolysis and subsequent gas-phase reactions of nylon. Further, the mass-loss rate of the model-fuel in the simulations was lower compared to the actual mass-loss of nylon in the experiments. This was necessary to achieve the same total HRR from the fuel in the simulation as in the experiments. There are further some additional, not as obvious, limitations of the model.

The flamelet model assumes fast chemistry and therefore describes the flaming region best. As such, it is important to model the flame region carefully. Generally the flamelet model needs a finer mesh compared to the other more commonly used combustion model, the eddy break-up model, in order resolve the single chemical species formation in space and time. Thus, especially in the fire region and in the vicinity of it, the grid cell size of a few centimetres gives very different results in chemical species concentrations to that of cell sizes of a few decimetres.

The fast chemistry approach that the flamelet model is based on is not possibly the best in describing the formation of some species with slower kinetics, such as NOx and soot. The faster the chemistry the more valid is the flamelet concept.

As one route of the HCN formation is via NOx, the fast chemistry approach might not be entirely correct in describing the HCN kinetics. This might thus affect the calculated

concentrations of HCN in this study. For calculation of slow kinetics the flamelet model could possible in the future be modified to take account of the residence time of species.

Preparatory calculations in this study showed that a cell size of two centimetres in the fire region was necessary to obtain reasonable resolution of the species. The chemical reactions also occur in other regions in the compartment, such as in the hot gas layer. In this study, somewhat larger cells were used in the hot gas layer region. This may have influenced the results if the combustion has in reality been occurring in the gas layer. This could explain the somewhat lower temperatures in the gas layer.

The results of this work show that there is large difference in the calculated species concentrations when using different flamelet options. The non-vitiated case produced low concentrations of both CO and HCN, compared to vitiated case. In particular, the HCN concentration at the opening flow was nearly 10 times lower when calculated using the non-vitiated option than using the vitiated option. The vitiated option proved to be more correct relative to the measurements. Therefore, when simulating a certain scenario, one should take into account whether the air in the entrainment region to fire is vitiated or not.

During the first minutes after the fire ignition, the air near the fire location is non-vitiated. The length of the time to vitiation depends on the room and fire size in relation to the ventilation. Once air in the entrainment region has become vitiated the vitiated flamelets should be used. The flamelet option from non-vitiated to vitiated must be switched manually in the current version of SOFIE. The current model includes eight levels of vitiation, i.e. totally 17 sets of flamelets for each species including 30 radiation levels. Thus, the flamelet lookup tables are so large that one value of vitiation allocates about 500 Mb of computer memory. Having all the vitiation levels in the computer memory at same time would need nearly 10 Gb of memory.

Although this study shows some weaknesses in the application of the model-fuel for a solid fuel and further in some assumptions of the model, the results of the simulations are encouraging, and prove that the model is capable of qualitative prediction and that the model approach should be validated further for other scenarios and fuels.

9 Future work

As the results show that the formation of HCN can be approximately predicted using the laminar flamelet model of the nitrogen-containing model fuel connected to a CFD model, a question arises: is this method usable to calculate the formation of other nitrogen species in fires? The answer is both yes and no. All species, including all intermediate products of combustion involved in the chemical reaction mechanism used, could be connected in the CFD flow field calculations. The user must do some programming to connect the new species into his CFD.

There is no practical interest to have intermediate species in the CFD flow field presentations. Their influence of the total chemistry and enthalpy are however included in the calculation. For example, the user has no interest in the distribution of OH, O and H radicals, even though they are necessary for combustion. Further, all the calculated parameters that the CFD model displays, such as chemical species, temperature, enthalpy, pressure, etc. are given as mean values of the actual time step chosen. The OH, O and H radicals, exist only in isolated regions, in the flame sheets, so their total concentrations are very low compared to the main species. Thus, to display these species would not give the user any valid information about distribution pattern in the space. To be able to display these species distribution the control volumes and times steps would have to be very small, in the order of one-tenth of a millimetre and a millisecond, respectively.

Other nitrogen containing species from fires that would be of interest to study are NH_3, NO and NO_2 as all of these species give a contribution to the total toxicity of the fire gases. It would further be of interest to study the factors governing the production of isocyanate acid (HNCO), as this species has recently been found from the combustion of many nitrogen-containing materials, e.g. particleboard and melamine [31].

To implement these species into SOFIE the flamelet state relationships from the flamelet calculation conducted in this project can be used. The only work needed is the coding in the computer program to put the new species in its “own place” in the program, thus no calculation of a new set of flamelets is necessary.

There are however other species that could be interesting to implement into CFD, such as hydrogen chloride, HCl. This species is not only toxic for humans to inhale, but it is also corrosive, i.e. it destroys metallic components in our environment. HCl is formed e.g. in combustion of poly vinyl chloride (PVC), for example in fires of electrical cables. The modelling technique to implement the formation of HCl should possibly be other than flamelet modelling, due to its production behaviour. One alternative is to implement HCl as a mass source that emits HCl corresponding to the mass flow of the fuel. The levels of HCl yield could be taken from laboratory measurements, e.g. from cone calorimeter measurements. Thus, the chemical reaction mechanism of the formation of it would not be necessary. However, it would probably be necessary to include some correction term for loss of HCl due to deposition on surfaces etc.

In order to have all pre-calculated vitiation data available for the flow field calculations, the flamelet model should be modified by including an additional dimension (vitiation fraction). However, the computer memory demand would be so large that we must wait for the next generation’s PC in lieu of large supercomputers available. Another approach is to use the flamelet calculations interactively at the same time as flow field calculations, using so called representative interactive flamelets.

In the calculated flamelet sets re-circulation with both cold and hot combustion gases was taken into account. However, in the preparatory CFD simulations presented in this report only vitiation with could combustion gases were investigated. Simulations with hot combustion gases should be investigated in a full validation of the model. Likewise, the effect of higher strain rates should be investigated.

Fuel 1 that was used in the CFD simulations of a nylon fire in this work showed promising results regarding predictions of trends in HCN formation. To investigate the generality of the model, Fuel 2 (with a lower nitrogen content) should be tested in a simulation of e.g. a fire including particleboard. It would further be interesting to combine the flamelet-model developed here with a flame-spread model for an assessment of the CFD tools capability to capture all aspects of a room fire, i.e., fire growth, fire spread and toxicity.

10 References

[1] Simonson, M., Tuovinen, H., and Emanuelsson, V., ”Formation of Hydrogen Cyanide in Fires”, A Literature and Experimental Investigation, SP REPORT 2000:27.

[2] Spalding, D. B., ”Mixing and Chemical Reaction in Steady Confined Turbulent Flames”, *Thirteenth Symposium (International) on Combustion.* The Combustion Institute, Pittsburg, PA, pp 649-657, 1971.

[3] Liew, S, K., “Flamelet Models of Turbulent Non-Premixed Combustion, PhD thesis”, Southampton University, UK (1983).

[4] Cox, G, “Combustion Fundamentals of Fire”, Academic Press, London, 1995.

[5] Tuovinen, H., ”Application of Flamelet Chemistry Model to Vitiated Methane-Air Diffusion Flames”, Department of Fire Safety Engineering, Lund University, Report, LUTVDG/TVBB3065-SE, 1992.

[6] Tuovinen, H. ”Modelling of Laminar Diffusion Flames in Vitiated Environment”, 4th International Symposium on Fire Safety Science, 13-17 June 1994, Ottawa, Canada.

[7] Tuovinen, H., “CFD Modelling of Under-Ventilated Fires”, SP REPORT 1996:41.

[8] Tuovinen, H. ”CFD modelling of Under-Ventilated Fires”, Fire-and-Explosion Hazard of Substances and Venting of Deflagrations- Proceedings of the Second International Seminar, All-Russian Research Institute for Fire Protection and Russian Association For Fire Safety Science, Moscow, Russia, 1997.

[9] Tuovinen, H. And Simonson, M., ”Incorporation of Detailed Chemistry into CFD Modelling of Compartments Fires”, SP REPORT 1999:03.

[10] Tuovinen, H. and Simonson, M. ” Incorporation of Detailed Chemistry into CFD Modelling of Compartment Fires”, The Third International Seminar on Fire and Explosion Hazards”. University of Central Lancashire, Lake Windermere, English Lake District, UK, (2000).

[11] Mauss, F. and Balthasar, M., Personnel communication, Lund Institute of Technology, Department of Combustion Physics, 1997.

[12] Magnussen, B. F., *The Eddy Dissipation Concept,* XI Task Leaders Meeting - Energy Conservation in Combustion, IEA, 1989.

[13] Bressloff, N. W., Moss, J. B. and Rubini, P., A., ”Assessment of a Differential Total Absorptivity Solution to the Radiative Transfer Equation as Applied in the Discrete Transfer Radiation Model”, Numerical Heat Transfer, Part B, 29: pp 381-397, 1996.

[14] Lewis, M. J., Moss, J. B. And Rubini, P. A., ”CFD modelling of Combustion and Heat Transfer in Compartment Fires”, Fire Safety Science - Proceedings of the

Fifth International Symposium, Melbourne, 1977.

[15] Bengtsson, L. G., Gustavsson, S., Tuovinen, H. and Werling, P., ”Experiment at the Cardington Large Building Test Facility”, Brandforsk project no 746-961, SP AR 1997:15, Borås 1997.

[16] Van Hees, P., Tuovinen, H. and Persson, B., ”Simulation of the Switel Hotel Fire”, Swedish National Testing and Research Institute, Fire Technology,SP-AR 1997:xx, Borås 1997.

[17] Williams, F.A., Combustion Theory, Second Edition, Addison-Wesley Publishing Company, Menlo Park, CA 1985.

[18] Peters, N., Prog. Energy Combust. Sci. 10:319-339 (1984).

[19] Lönnermark, A., Blomqvist, P., Månsson, M. and Persson, H., TOXFIRE – Fire Characteristics and Smoke Gas Analysis in Under-Ventilated Large-Scale Combustion Experiments, Tests in the ISO 9705 Room, SP-REPORT 1996:45.

[20] Lönnermark, A., Babrauskas, V., TOXFIRE – Fire Characteristics and Smoke Gas Analysis in Under-Ventilated Large-Scale Combustion Experiments: Theoretical Background and Calculations, SP-REPORT 1996:49.

[21] Blomqvist, P., P. Lindberg, and M. Månsson, *TOXFIRE-Fire Characteristics and smoke Gas Analysis in Under-ventilated Large-scale Combustion Experiments: FTIR Measurements*. SP REPORT 1996:47. 1998, Borås: SP Swedish National Testing and Research Institute

[22] Kantak, M. V., De Manrique, K. S., Aglave, R. H. and Hesketh, R. P., “Methylamine Oxidation in a Flow Reactor: Mechanism and Modeling”, *Combustion and Flame* **108**: 235-265 (1997).

[23] Hjuler, K., Glarborg, P. and Dam-Johansen, K., *Ind. Eng. Shem. Res*.,**34**:1882 (1995).

[24] Basevich, V. Ya., Kogarko, S. M. and Tyurin, A. M., *Khim. Fiz.,* **2(1)**: 113 (1983).

[25] Fenimore, C.D., *J. Combust. Flame*, **19**:289 (1972).

[26] Bowman, C.T., in Fossil Fuel Combustion – A source Book (W. Bartok and A.F. Sarofim, Eds.), John Wiley, New York, 1991, p. 314.

[27] Glassman, I., Combustion (3rd edition), Academic Press Inc., San Diego, 1996.

[28] Braun, E. and Levin, B.C., *Fire and Materials*, **11**, 71-88 (1987).

[29] Leichtnam, J.-N. et al., *Journal of Analytical and Applied Pyrolysis*, **55**, 255-268 (2000).

[30] Conway, D.C. and Marak, R., *J. Polym. Sci. Polym. Chem.*, **20**, 1765-1775 (1982).

[31] Hertzberg, T., Blomqvist, P., Dalene, M., Skarping, G., ”Particles and isocyanates from fires”, SP-REPORT 2003:05.

Appendix A

Figures A1 to A3 show the calculated temperature field and concentrations of HCN, CO and CO_2 at the room centreline. Figure A4 shows the computer model of the room used in simulations.

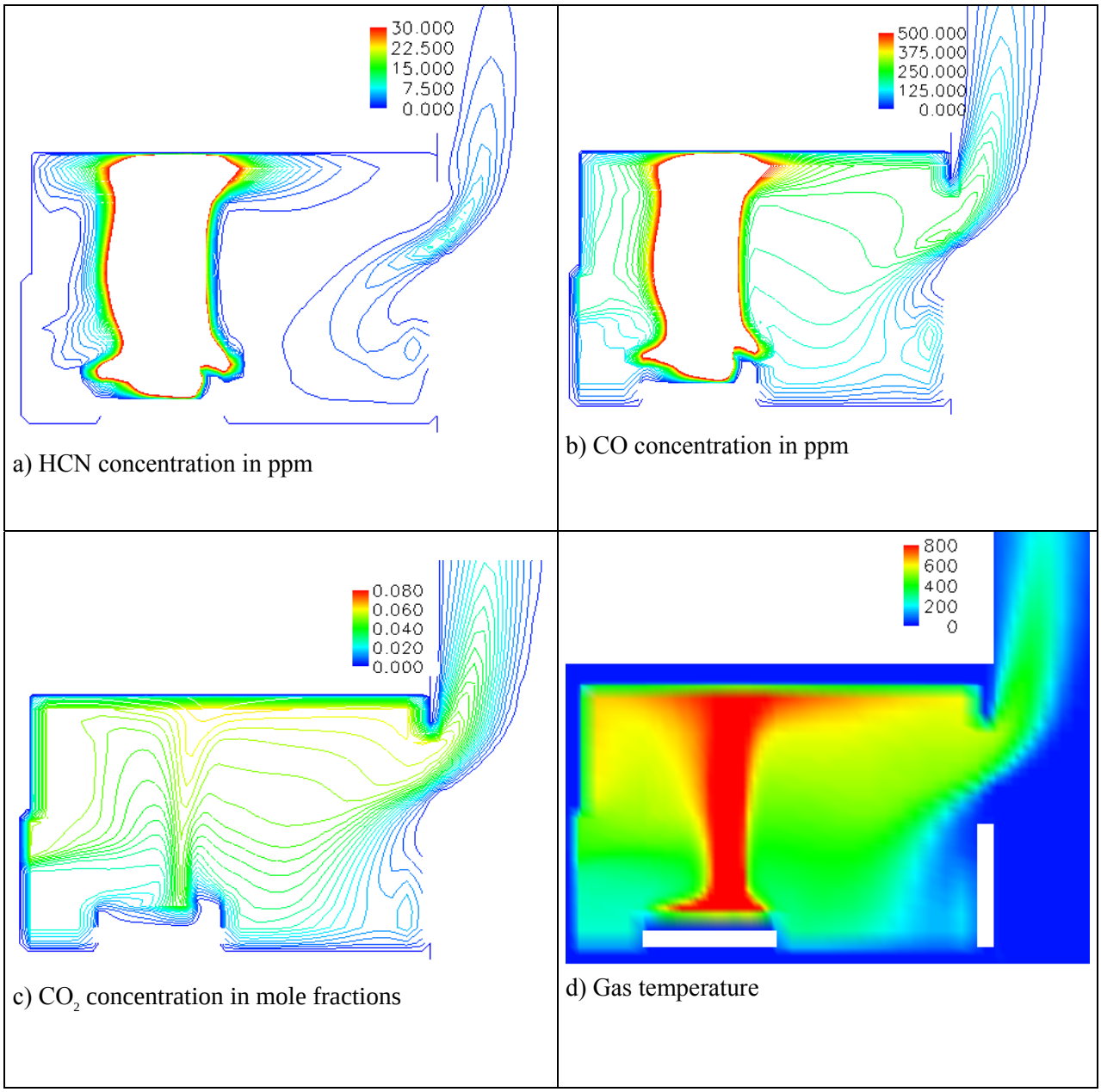

a) HCN concentration in ppm

b) CO concentration in ppm

c) CO_2 concentration in mole fractions

d) Gas temperature

Figure A1. Calculated species concentration of a) HCN, b) CO and c) CO_2. d) Calculated temperature. Non-vitiated flamelets used. Opening height 0.89 m.

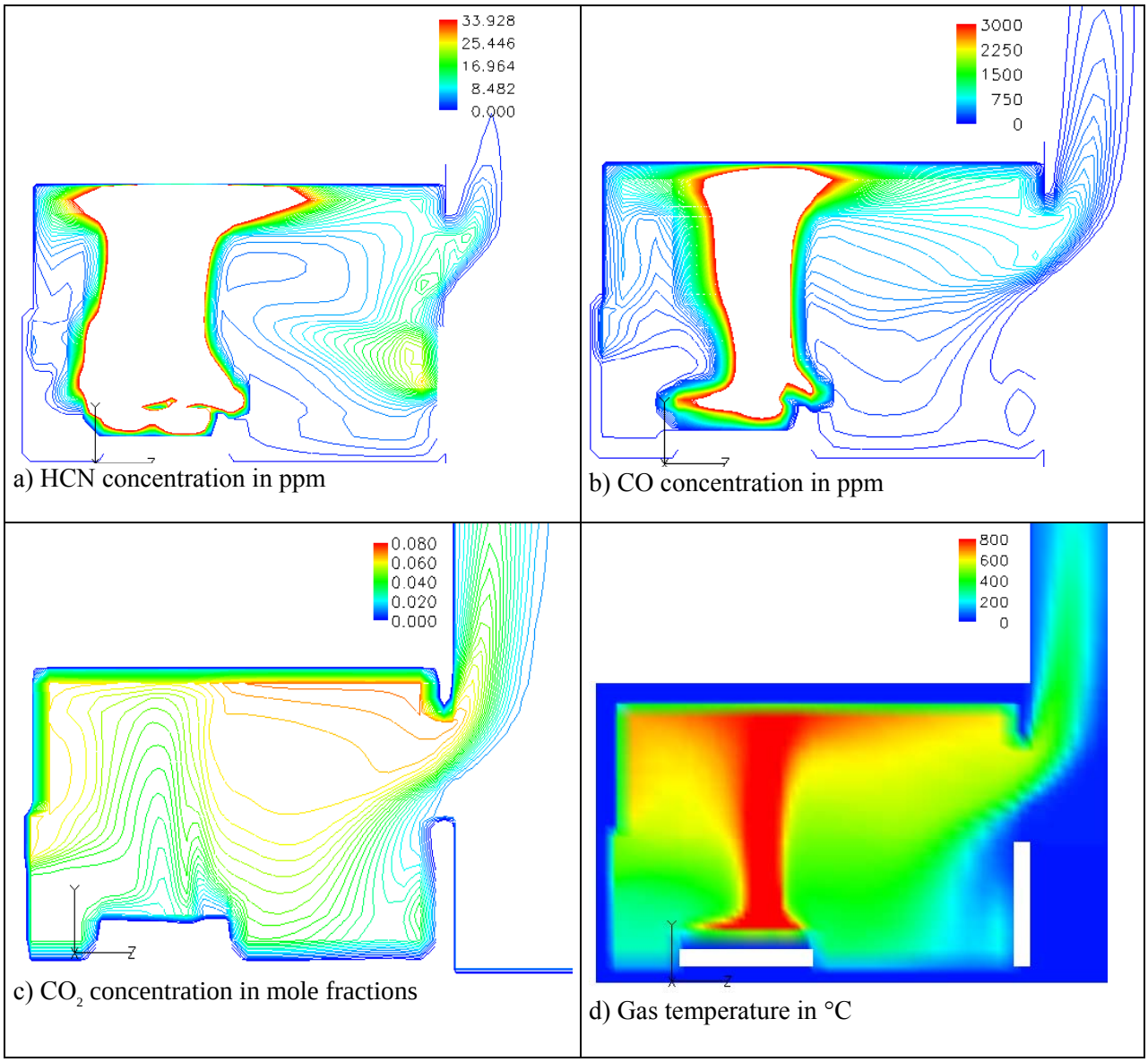

Figure A2. Calculated species concentration of a) HCN, b) CO and c) CO_2. d) Calculated temperature. Vitiated flamelets used. Opening height 0.89 m.

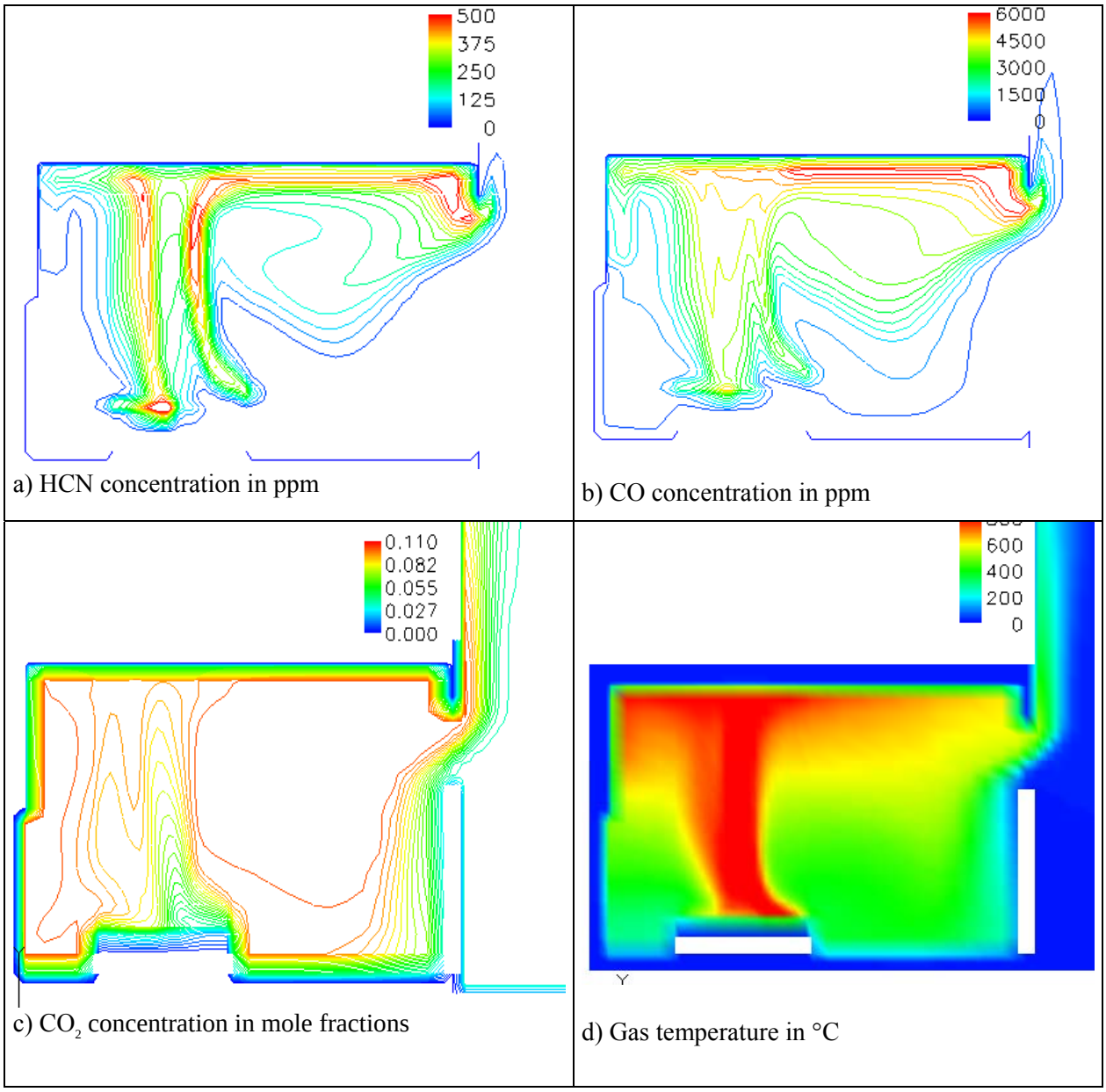

a) HCN concentration in ppm

b) CO concentration in ppm

c) CO_2 concentration in mole fractions

d) Gas temperature in °C

Figure A3. Calculated species concentration of a) HCN, b) CO and c) CO_2. d) Calculated temperature. Vitiated flamelets used. Opening height 0.56 m.

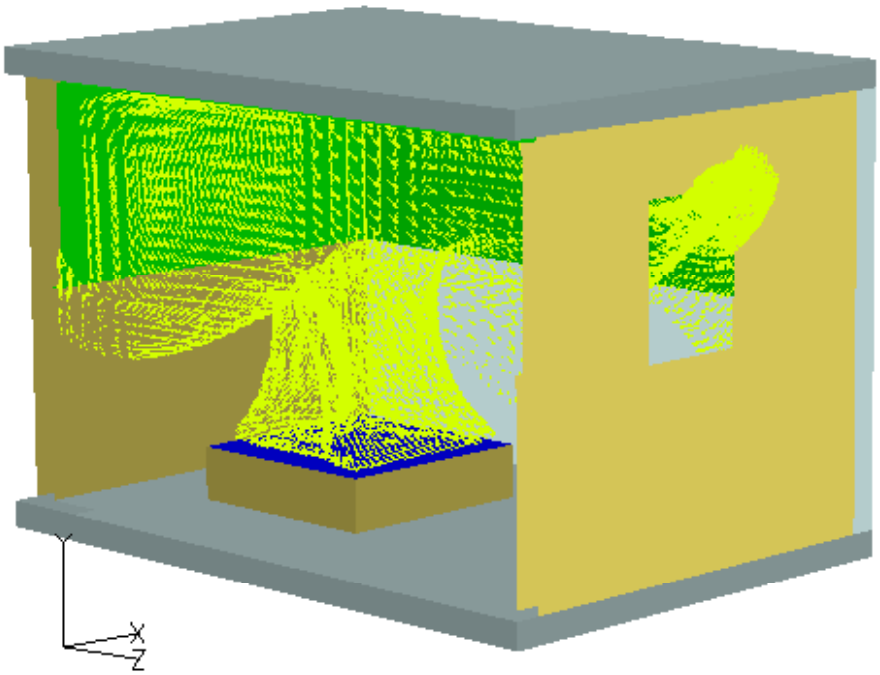

Figure A4. A sketch of the computer model of the room used in the simulations. The arrows show the direction of gas flow on the iso-surface for temperature 600℃. Opening height is 0.89 m.

Appendix B

Figures B1 to B3 show flamelet concentration data for HCN and temperature (a) – (b) respective (c) – (d), CO (e) and CO_2 (f) for some selected combustion conditions. Figure B 4 shows flamelet data for HCN and temperature for hot and cold vitiation compared for different degrees of radiation losses.

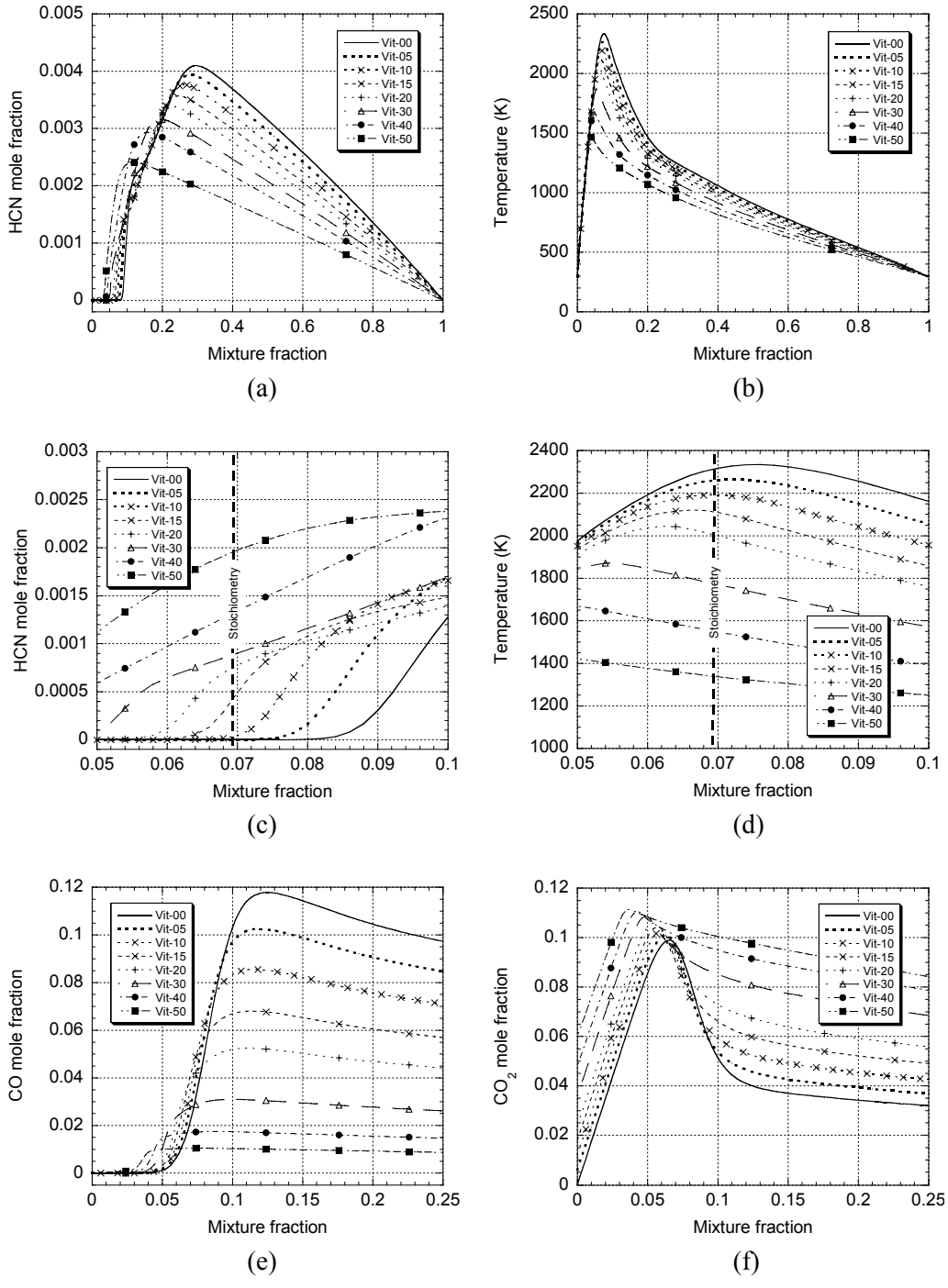

Figure B1. Flamelet data for varying degrees of (cold) vitiation, no radiation losses.

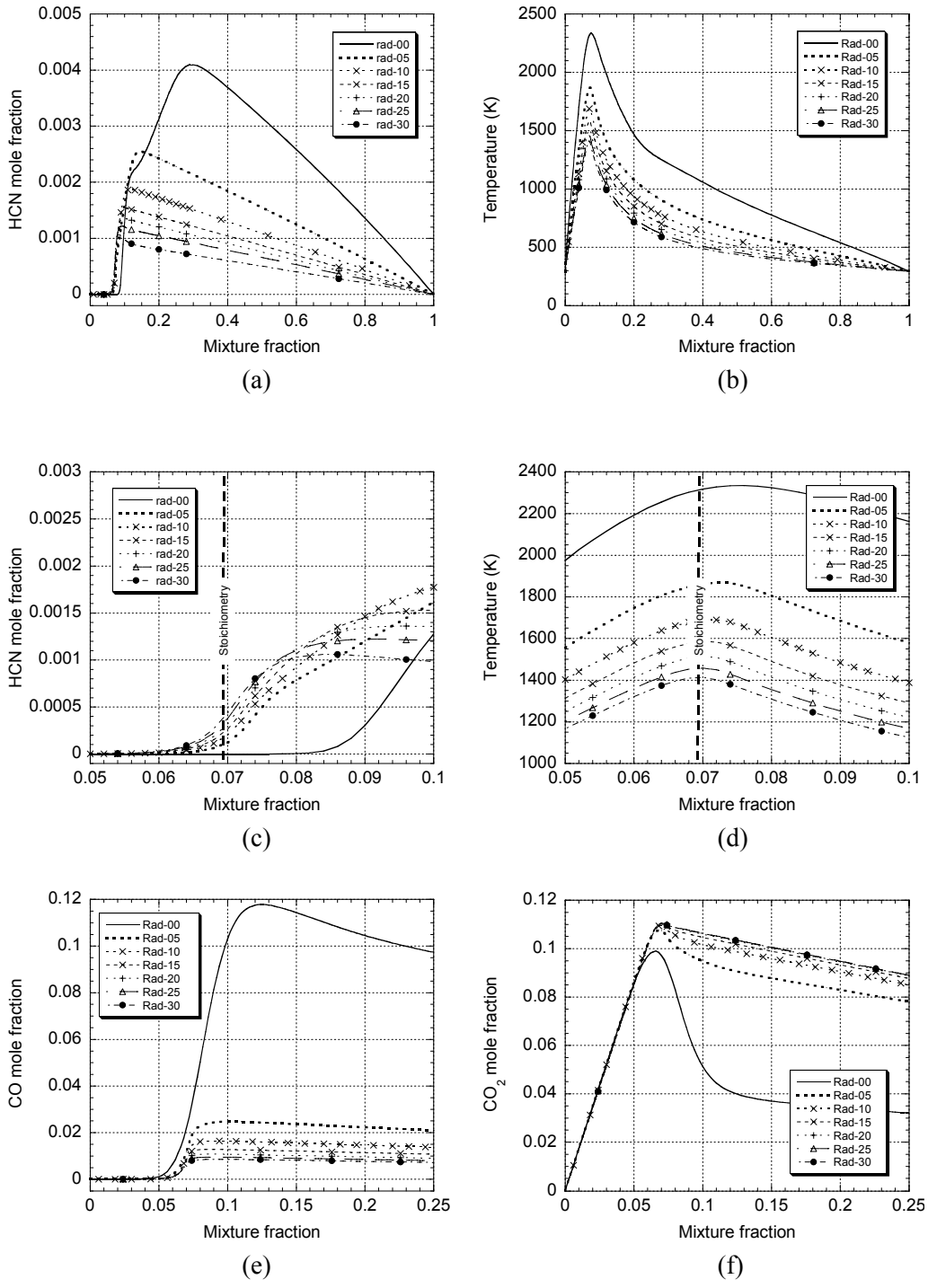

Figure B2. Flamelet data for varying degrees of radiation losses, no vitiation.

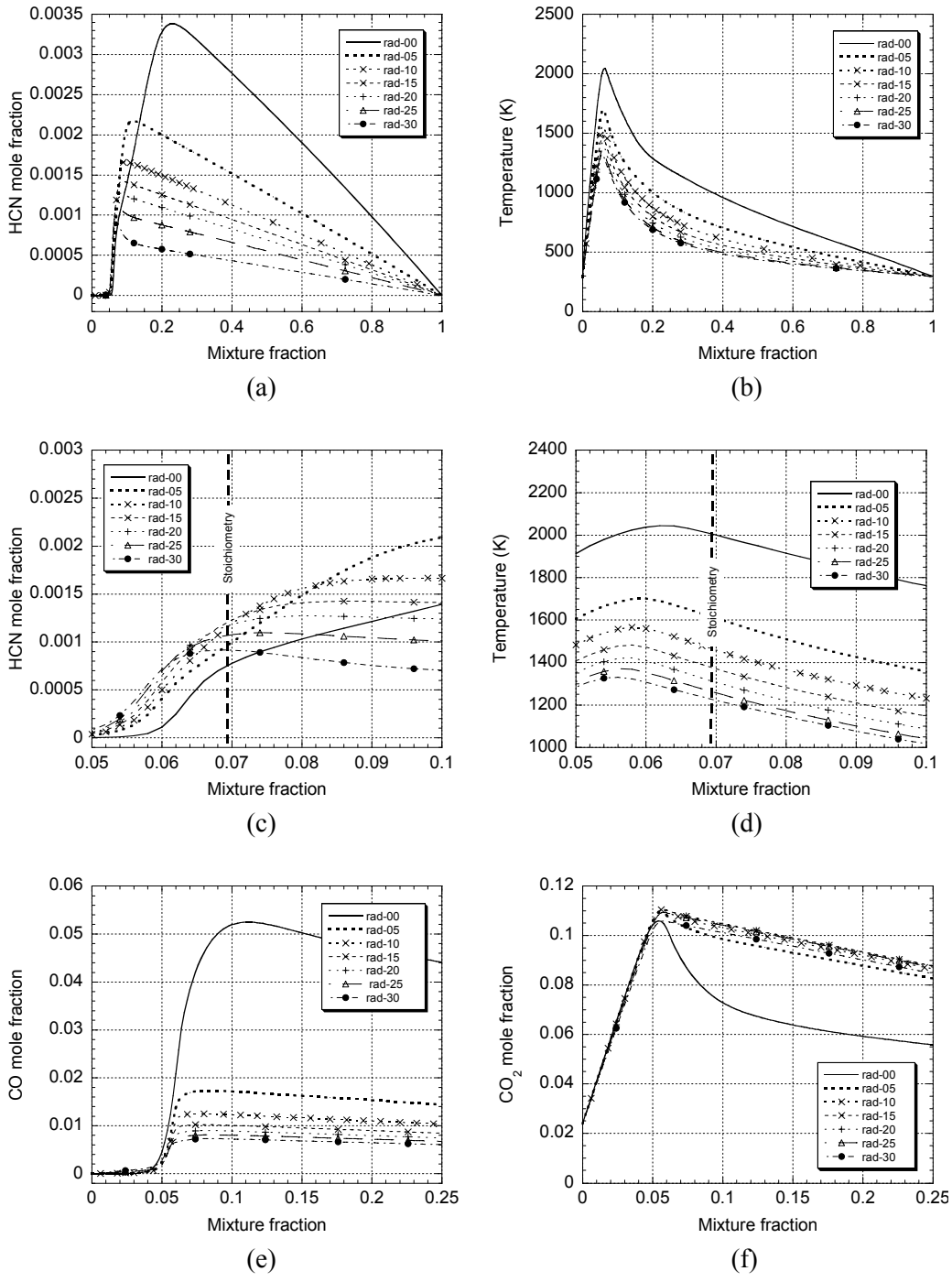

Figure B3. Flamelet data for varying degrees of radiation losses, (cold) vitiation 20 %.

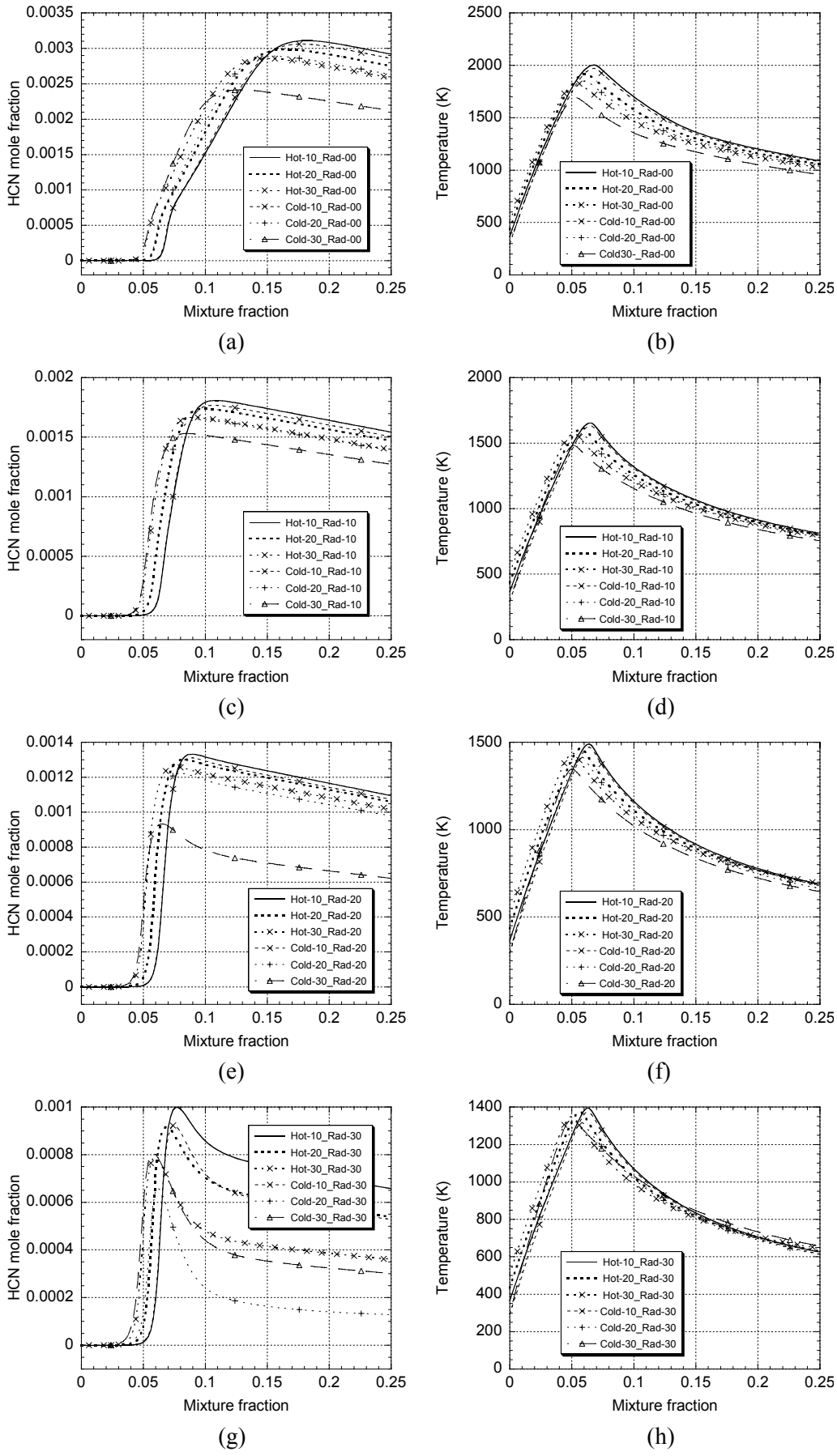

Figure B4. Flamelet data for HCN and temperature. Comparison of hot and cold vitiation with varying degrees of radiation losses.